

SRNL | LDRD Annual Report

2011



SRNL
SAVANNAH RIVER NATIONAL LABORATORY

We Put Science To Work™

From the Laboratory Director



I am pleased to introduce the 2011 Laboratory Directed Research and Development (LDRD) Annual Report. This important program displays both the breadth of SRNL's research efforts and the depth of our commitment to expand the capability and mission impact of this Laboratory. We continue to broaden participation in the LDRD program across the Laboratory while maintaining our record of innovative technical accomplishment.

In 2011, the initial group of Strategic Initiatives, which started in late FY09, ended their two year funding period. The projects were successful in spurring new technological capabilities and expertise at SRNL and strengthening our scientific and technical foundation. As evidence of success, the projects yielded numerous peer-reviewed publications and patent applications, strengthened university collaborations, and supported post-doctoral participation. By the close of FY 2011, two of the four projects had secured follow-on external funding, the end-goal for LDRD projects.

The new projects started in 2011 included 14 Standard projects and three Strategic Initiatives. Many of these projects led to publishable results and patent applications within the year. A team lead by Robin Brigmon demonstrated that cooling towers could serve as collection platforms for airborne particulate biological targets. Robert Buckley and co-workers developed evolutionary programming techniques to create meteorological datasets that outperform the standard initial conditions ensemble for the southeast United States for the spring and summer months studied in this research. Stephen Garrison headed an effort to design, fabricate and test a gadolinium based solid-state neutron detector, which yielded an invention disclosure.

The scientific and engineering progress described in this Annual Report will provide the foundations for future programs that will help SRNL maintain its position as DOE's premier applied science and engineering laboratory. SRNL's researchers have again shown that the LDRD program is a sound investment by the Laboratory that will pay dividends to both the Laboratory and the nation in the future.

A handwritten signature in black ink, appearing to read 'T Michalske', written in a cursive style.

Dr. Terry Michalske

Table of Contents

Project Titles, *Investigators*

FY 2009 Strategic Initiative Project Summaries	1
Advanced Batteries for Electric Energy Storage, <i>M. Au, E. Fox, H. Colon-Mercado</i>	1
Development of High Capacity Portable Power Systems, <i>T. Motyka, R. Zidan, K. Heung, J. Teproovich, D. Knight, and L. Dinh</i>	2
Nanosized Titanates for Optimized Performance in Separations Science, Innovative Medical Applications and Photochemistry, <i>D. T. Hobbs, M. C. Elvington, M. H. Tosten, K. M. L. Taylor-Pashow (SRNL); J. Wataha (U. Washington); M. D. Nyman (SNL)</i>	4
The Use of Statistical Downscaling to Project Regional Climate Changes as They Relate to Future Energy Production, <i>D. W. Werth, K.F. Chen, A. Garrett, S. Aleman, B. L. O'Steen, and M. Altinakar</i>	6
FY 2011 Strategic Initiative Project Summaries	8
Nano-Photocatalysts for Solar Fuels Applications: Conversion of CO ₂ to Hydrocarbons, <i>S. Hunyadi Murph, K. Heroux, T. Sessions, R. Lascola, B. Peters, Y. Zhao (UGA), S. Ullrich (UGA), A. Greytak (USC), S. Retterer (ORNL)</i>	8
Reactive Gas Recycling of Used Nuclear Fuels, <i>J. Gray, P. Korinko, M. Martinez-Rodriguez, S. Sherman, R. Torres, B. Garcia-Diaz, G. Morgan, A. Visser, T. Sudarshan, and T. Adams</i>	10
Risk Reduction and Process Optimization for Engineered Algae Production Systems, <i>Michael Heitkamp, C. Bagwell, C. Yeager, S. Sherman, C. Berry, C. Milliken, T. Soule, K. Sander, R. Barrier, M. Piskorski(USCA), P. Moeller(NOAA), P. Zimba (Texas A&M)</i>	13
FY 2011 Standard Project Summaries.....	14
Advanced Gas Sensors Using SERS-Activated Waveguides, <i>R. Lascola, S. Murph, J. Reppert, K. Heroux, S. McWhorter</i>	14
Application of Cooling Towers for Collection, Concentration, and Detection of Biological Agents, and Elemental Chemicals, <i>R. L. Brigmon, M. T. Kingsley, W. L. Jones, S. Leskinen (University of South Florida), E. Kearns (University of South Florida) & D. Lim (University of South Florida)</i>	17
Can Ionic Liquids be used as Templating Agents for Controlled Design of U-Containing Nanomaterials?, <i>A. Visser, N. Bridges, and A. Duncan</i>	19
Carbon Nanomaterials with Encapsulated Gadolinium for Advanced Neutron Detection, <i>S.L. Garrison, L. C. Teague, J. R. Coleman, T. B. Brown, M.R. Kriz</i>	21
Charge Transport and Storage in Organic Semiconducting Materials: Toward Improved and Future Device Structures, <i>L. C. Teague</i>	23
Detoxification of Uranium in Soils and Groundwater Using Recycled Concrete, <i>M. Denham, B. Jones, A. Knox, and M. Whiteside</i>	24
Establishing the Potential of the TERAS System for CO ₂ Capture and Sequestration, <i>M. B. Gorenssek, M. A. Shadday, G. C. Blount</i>	26

Extraction of Hemicellulose and Lignin from Biomass, <i>S. R. Sherman, A. Womack, and J. Goodell</i>	29
Heterogeneous Materials and Novel Interfaces for Oxygen Separation Membranes, <i>K. Brinkman (SRNL), K. Reifsnider (USC) and A. Virkar (Univ. Utah)</i>	30
High Performance Nanofluidic Sensors for Detecting Chemical and Biological Agents in Deterrence of Terrorist Attacks, <i>P.S. Lam, A. Méndez Torres, R. Torres, D. Hathcock, Prof. G. Wang (USC)</i>	32
Improved Characterization of Air Emission Sources Using Evolutionary Ensembles, <i>R.L. Buckley, S. R. Chiswell, D.W. Werth, and B. L. O'Steen</i>	34
Ionogels as Solid Electrolytes for Advanced Battery Applications, <i>B. Garcia-Diaz, J. Gray, A. Visser, M. Au, J. Weidner, K. Zeigler, and T. Adams</i>	36
Organic-based Ionic Salts for the Optimization of Alkaline Fuel Cells, <i>E. B. Fox (PI), H.R. Colón-Mercado, A.E. Visser, N. J. Bridges, C. W. James, and W. Ho (Ohio State)</i>	38
Stable Electrocatalysts for High Temperature Fuel Cells, <i>M. C. Elvington, H. R. Colón-Mercado</i>	41

2011 Laboratory-Directed Research and Development Program Annual Report

FY 2009 Strategic Initiative Project Summaries

Advanced Batteries for Electric Energy Storage, M. Au, E. Fox, H. Colon-Mercado

This research resulted in the development of advanced batteries with high capacity, low cost and inherent safety for electric energy storage. The research activities consisted of two parts. 1) Li/air batteries focusing on rechargeability; 2) Li-ion batteries using nanostructured Si anodes focusing on capacity retention.

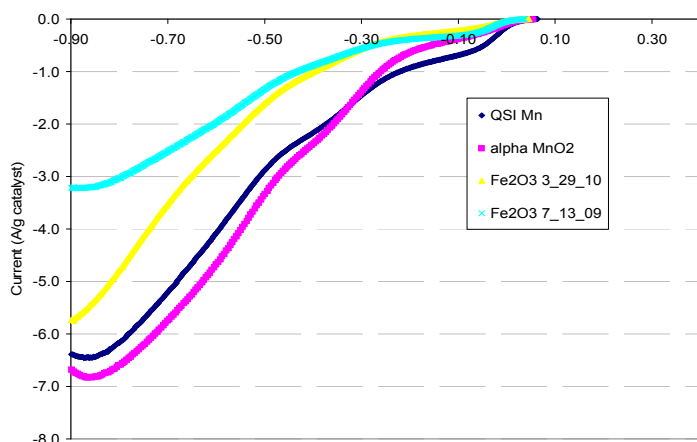


Figure 1. Linear sweep voltammetry of un-supported catalysts at 800 rpm and in 0.1 M LiOH saturated with O₂.

The results show that the Li/air batteries using polymer electrolytes has poor rechargeability due to reaction with discharge products and high vapor pressure leading cell dry-out. Seven ionic liquid (IL) based electrolytes were developed and evaluated. It shows that the rechargeability the Li/air batteries using IL was improved. A multilayered Li/air battery using hybrid electrolyte of PC/IL and α -MnO₂ nanotubes catalyst demonstrated the capacity of 600 mAh/g in 50 cycles.

However, only the portion of lithium oxides able to access the catalysts can be reduced. The rest lithium oxides will be accumulated in the pores of the cathodes and eventually clog the pores resulting in oxygen deficiency and gradual decrease of capacity (Fig. 2).

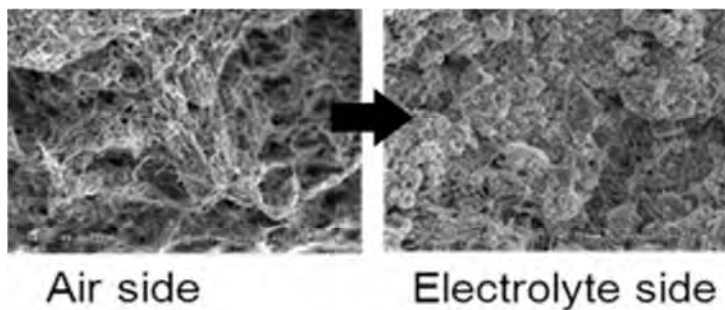


Figure 2. The pores in cathode are clogged by lithium oxides after 50 cycles

For this reason, the cycling life of our Li/air batteries using IL based electrolytes is less than 50 cycles. To extend the cycling life for hundred or even thousand cycles, the fundamental changes in air cathode structure and electrolyte selection are needed.

Although Si anodes show very high capacity (theoretically 4100 mAh/g), it is not sustainable due to huge volume change and materials pulverization during charge-discharge cycles. To retain the high initial capacity, the Si-Cu composite nanorods were synthesized. The in-situ TEM/AFM experiments show mechanical flexibility and structure stability of Si-Cu composite nanorods. The Li-ion batteries with Si-Cu composite anodes demonstrated the capacity of 600 mAh/g in 100 cycles (Fig. 3).

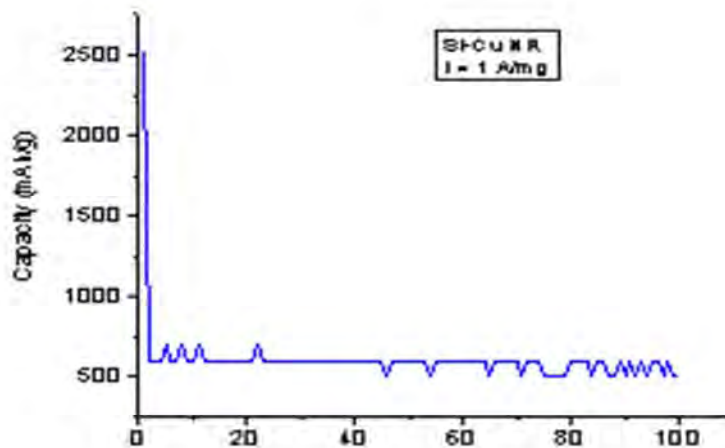


Figure 3. The cycling capacity of Si-Cu composite nanorods anode

Development of High Capacity Portable Power Systems, T. Motyka, R. Zidan, K. Heung, J. Teprovich, D. Knight, and L. Dinh

The specific energy densities of today's best batteries vary from 150 Wh/kg for secondary Li batteries to less than 400 Wh/kg for primary Li batteries. The DoD and commercial portable equipment manufacturers are requesting specific energy densities greater than 1000 Wh/kg – more than 2 to 3 times that of the best primary Li batteries today. Hydrogen with the highest energy density of any fuel at 33,000 Wh/kg has the greatest potential to meet this goal. A team at SRNL has been working on the development of such a high energy density portable powered systems based on aluminum hydride or alane, a light-weight, high capacity solid-state hydrogen storage material. The specific accomplishments of our project included 1) the development of a new patent-pending process to reduce the cost of producing alane 2) the demonstration of a new two-step hydrogen delivery process from alane, which has the potential to produce twice as much energy and 3) the successful design, fabrication and operation of an alane-based hydrogen storage vessel and integration of the vessel with a 150 watt commercial fuel cell.

SRNL has been working on developing several light-weight, high capacity solid-state hydrogen storage materials. One of the most promising materials is aluminum hydride, (AlH₃) or alane. Alane, while not a new material, has only in the last few years been considered as a hydrogen storage material for fuel cell applications. SRNL researchers are among only a handful of researchers, worldwide, currently working with alane and beginning to unwrap its material and engineering properties. The specific objectives of this project were: 1) to characterize and optimize

alane as a novel new hydrogen storage material 2) to develop a small hydrogen storage vessel containing alane and to demonstrate hydrogen release and delivery rates suitable to power small commercial fuel cells and 3) to provide sufficient data and interest to develop additional military and commercial initiatives.

DOE has invested numerous years and millions of dollars to develop advanced hydrogen storage materials for automotive applications. Many of these materials have demonstrated very high hydrogen capacities (greater than 20 percent by weight) but most do not meet all the various requirements needed for automotive applications. Many of these materials, however, may be viable for small portable power systems. The goal of this research is to develop small power systems (2-3 X better than today's best battery technology) around novel advanced hydrogen storage materials coupled with small fuel cells and other hybrid technologies.

At the present time only a limited amount of commercial alane is readily available. As part of this project a new supplier of alane was identified to provide sufficient quantities of alane needed to carry out this project. Also as part of this project a bench-scale system was developed to produce quantities of alane for experimental and optimization studies. During the course of this work a new and potentially lower cost process for producing alane was developed. The novel process minimizes the use of solvents and is able to produce very pure halide free alane. An invention disclosure was submitted and a provisional patent is being filed.

For some military and commercial applications it has been shown that water can be used to produce hydrogen by its reaction with various metals like aluminum. One of the problems with this method has been that the reaction with water often forms a gelatinous hydroxide which coats the aluminum and limits the extent of reaction and the amount of hydrogen released. A series of tests were performed to evaluate both alane and the spent aluminum byproduct in aqueous reactions both with and without additives to enhance the amount of hydrogen that can be released. We were able to demonstrate a novel two step process, which first desorbs the hydrogen from the alane by heating and then a second step, which adds a stoichiometric amount of water to liberate additional hydrogen. A patent application and a paper have been submitted for this process, which has been found to produce two times the amount of hydrogen compared to a single step process.

A major part of this project was to evaluate alane systems for compatibility with small fuel cell applications. Preliminary results on a proof-of-concept vessel containing approximately 22 grams of alane showed that the system could scale nicely to meet the required hydrogen release rate for a small 100 W fuel cell system. Based on those results a larger system containing 240 grams of alane was designed, fabricated and tested with a 150 watt commercial fuel cell. The results show that the system was able to operate the fuel cell at near full power for over two hours and at reduced power for several more hours. The demonstration showed that high-specific-energy portable power systems based on alane and other high capacity metal hydrides are possible and that this research can lead to further development of future portable power systems that meet not only DoD but commercial customer needs.

Two patents are already being pursued from this work and more may be forthcoming. Several papers have been submitted and more are being planned. Perhaps the largest accomplishment of

this project is the interest obtained from several commercial companies working in the area of portable power systems. Additional funding from DOE EERE has already been secured this year with more potential funding next year for SRNL to pursue a CRADA with at least one commercial company for alane material development for portable power applications.

Nanosized Titanates for Optimized Performance in Separations Science, Innovative Medical Applications and Photochemistry, D. T. Hobbs, M. C. Elvington, M. H. Tosten, K. M. L. Taylor-Pashow (SRNL); J. Wataha (U. Washington); M. D. Nyman (SNL)

Three synthetic methods have been employed to produce nanosize alkali metal titanates. Method 1 utilizes a sol-gel technique coupled with a surfactant to produce spherically-shaped particles ranging from about 100 – 150 nm in size. Method 2 uses a delamination technique that produces fibrous particles that are about 10 – 20 nm wide and 100 – 500 nm in length. Method 3 is a hydrothermal technique previously reported in the literature and produces nanotubes having a diameter of about 10 nm and lengths of about 100 -500 nm. All of these materials were converted to the peroxotitanate form by reaction with hydrogen peroxide under mild conditions. Testing revealed that the materials function as effective ion exchangers, excellent photocatalysts for the decomposition of organic compounds, and effective platforms for the delivery of therapeutic metals.

Titanate materials are remarkably effective ion-exchange materials for the decontamination of radioactive and industrial wastewater solutions. For example, monosodium titanate (MST) is used at the Savannah River Site to remove radioactive strontium and alpha-emitting radionuclides (principally plutonium and neptunium isotopes) from high-level nuclear waste solutions. More recently, MST and the peroxide-modified MST, referred to as modified MST, or mMST, have been shown to be an effective platform for the delivery of biologically relevant metals to living cells under physiological conditions. MST and mMST are fine powders that are spherically shaped and are about 1 to 10 microns in diameter. The mMST is a bright yellow powder that is more photochemically active due to enhanced absorption of visible light.

Chemical and physical properties of solids can be significantly enhanced by increasing the surface area to volume ratio. For example, ion exchange rates are increased by increasing the available sites on particle surfaces and decreasing intra-particle transport distances. Similarly, catalytic properties are also enhanced by increasing the surface area relative to the total particle volume. Decreasing the size of solid particles is an effective strategy to increase the surface area to volume ratio. For example, a 10 nm particle has a surface area to volume ratio that is 1000 times that of a 10 micron particle. Thus, this project sought to synthesize titanate materials that feature nano-scale particle sizes (1 – 200 nm).

Three synthetic strategies were investigated to produce nanosize titanate materials. Method 1 utilizes a sol-gel technique similar to that used for the production of MST, but with different reagent concentrations and mixing methods coupled with a surfactant. Method 2 uses a delamination technique whereby micron size particles are unzipped to produce fibrous nanosize particles.

Method 3 is a hydrothermal technique previously reported in the literature that has been shown to produce nanotubes having a diameter of about 10 nm and lengths of about 100 -500 nm. After successfully synthesizing nanosize titanates we investigated ion exchange, photochemical and metal delivery properties for a variety of applications.

Nanosize sodium titanates with varying particle morphologies have been successfully prepared by three different synthetic techniques. Roughly spherically-shaped particles (Fig. 1A) ranging from about 100 – 150 nm in size were prepared by modifying the sol-gel method used to prepare MST. This method employed a non-ionic surfactant in combination with dilute reagent solutions to control particle size. A delamination technique produced fibrous particles (Fig. 1B) that are about 10 – 20 nm wide and 100 – 500 nm in length. Finally, a hydrothermal technique produced nanotubes (Fig. 1C) having a diameter of about 10 nm and lengths of about 100 -500 nm.

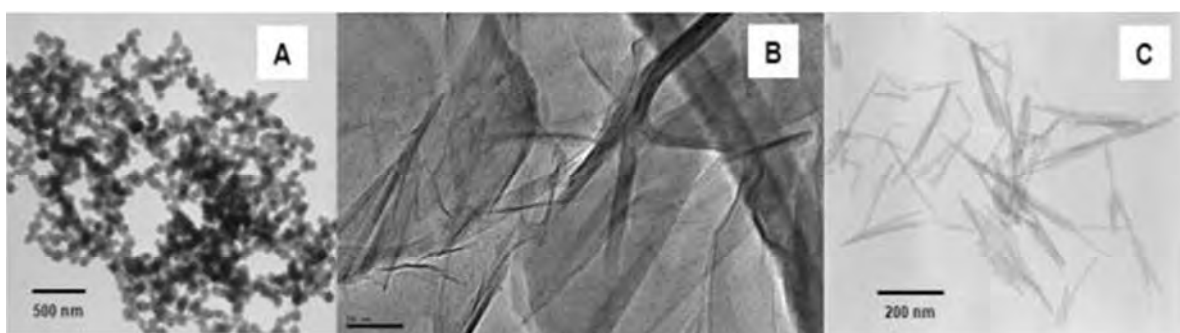


Figure 1. Transmission electron micrographs of nanosize titanates prepared by sol-gel (A), hydrothermal (B), and delamination (C) techniques.

All of these materials were successfully converted to a peroxotitanate form by reaction with hydrogen peroxide under mild conditions. As with micron-sized titanates, the peroxide-modified nanosize titanates exhibit a yellow color due to the η^2 -bound protonated hydroperoxo-titanium ligand-to-metal-charge-transfer absorption band at about 385 nm. The intensity of the yellow color is pH dependent and typically less intense with the nanotubes suggesting the chemically resistant surface of the nanotubes may limit conversion to the peroxo form.

Testing confirmed that the materials function as effective ion exchangers. For example, the nanoMST and nanotube samples, and their respective peroxide-modified forms, remove strontium and actinides (Pu, Np and U) when contacted with an alkaline salt solution simulating a SRS high-level waste supernate. Under weakly acidic conditions, the nanosize titanates and peroxotitanates removed more than 90% of 17 metal ions including alkaline earth, transition, heavy and main group metal ions. Furthermore, these materials also readily exchange Au^{3+} and Pt^{2+} ions for Na^+ ions when present in a pH 7.3 phosphate saline solution.

Peroxide and phosphate-modified delaminated titanates proved to be particularly good photocatalysts for the decomposition of organic contaminants. These materials exhibited improved photodegradation of two common dyes, bromophenyl-blue and methyl-orange, compared to a

commercial titanium dioxide catalyst indicating that these materials should serve as good catalysts over the pH range from about 4.5 to 9.

Screening in-vitro tests showed that both nano-size and micron-size metal-exchanged titanates inhibit the growth of a number oral cancer and bacterial cell lines. Metals investigated to date include Au(III), Au(I), Pt(II), Pt(IV), Pd(II), and Hg(II). The mechanism of inhibition is not known, but preliminary scanning electron microscopy results suggest that the titanates may be interacting directly with the wall of the nucleus to deliver sufficient metal ion concentration to the cell nucleus to inhibit cell replication.

Three synthetic techniques have been successful in producing nanosize titanates. The nanosize titanates exhibit good ion exchange characteristics, serve as photocatalysts for the decomposition of organic compounds, and are effective platforms for the delivery of therapeutic metals.

The Use of Statistical Downscaling to Project Regional Climate Changes as They Relate to Future Energy Production, D. W. Werth, K.F. Chen, A. Garrett, S. Aleman, B. L. O'Steen, and M. Altinakar

We develop a statistical downscaling process to global climate model (GCM) predictions of precipitation, temperature, and other climate variables through the use of both a scaling and a linear regression method. The downscaling technique involves the establishment of relationships between GCM data for the 20th century and observed data for the same period, and the application of the same relationship to 21st GCM predictions. This is done for several stations within a basin in northern Georgia, and this data is used to calculate future flow statistics for the upper Coosa river. Results are compared to historical Coosa River flow and to flows calculated with the original, undownscaled GCM data to determine if we might expect a reduced flow in the future. We have also applied this process to estimate the future ability of a North Carolina nuclear power plant and a Georgia coal-fired plant to adequately dissipate excess heat.

The objective of this study is to develop statistical downscaling to predict future water resources in the Southeast U.S. and apply the results to assess the impact on several modes of energy production. We selected a basin in northern Georgia that is subdivided into 4 sub-basins, as it plays an important role in supplying water for industry and domestic use in northern Georgia, and has been involved in water disputes in recent times. The basin also supplies cooling water for the 935MW coal-fired Hammond plant, which draws water from the Coosa river. The water is drawn through once and returned to the river directly from the generator (no cooling tower is used).

Predictions of greater precipitation bode well for future plant operations, but temperature increases could offset some (or all) of the benefit. We will simulate the future river flow of this basin using a watershed model forced with local climate data for the period 2040-2049, using future climate downscaled from a GCM as input to the model of the basin. This data will then be applied to a model of plant operations to estimate if the plant will require mitigating action to maintain operation.

The research utilized two methods for statistical downscaling of climate at various locations within the southeastern US. A scaling method is relatively straightforward, but has been shown to produce good recreations of 20th century statistics. Unlike other downscaling methods, it does not use the GCM large-scale data directly. Rather, it accepts as input the GCM gridded surface meteorological data (temperature and precipitation, which are related to the simulated large-scale data through the model parameterizations) interpolated to the desired observing station, along with actual data from the station for an identical time period to determine an appropriate 'correction' to the bias and variance of the GCM data to bring its statistics in line with the station data. This same correction is then applied to future predictors (GCM data for the 21st century).

The second method involves the linear regression of the pressure surface heights from the GCM onto the relevant climate variables. This was applied to observations from Raleigh, NC to establish the future ability of the Shearon-Harris nuclear plant to dissipate waste heat to the environment. (In this case, the climate variables were temperature and dewpoint.) The observed pressure heights from several levels were regressed onto the data from the station to obtain the linear coefficients, and this same linear relationship was applied to data from the GCM predictions for 2040-2049 to get the future temperature and dewpoint values.

For the basin simulation, runoff models for each of the four sub-basins were combined to form a single runoff model to simulate the upper Coosa River runoff flow for the entire basin upstream from Plant Hammond. The downscaled climate data were then used as input for the model to simulate river flow for the upper Coosa basin for the target 10-year period (2040-2049). The hourly meteorological data for the 2040s, derived from the 3 different global climate models (both scaled and unscaled), was used as input to create six predictions. A comparison of simulated flow data for the last 8 years of the 2040s (96 months) calculated for the scaled and unscaled data for each GCM shows that the effect of using the downscaled data is generally to increase the predicted flows over those calculated with the raw, unscaled GCM data.

The simulated flow frequency distributions shows that the simulated future flows are noticeably lower than the historical flows due to climate change. For example, the historic flows show a 1 in 20 chance of falling below 50m³/s, while the downscaled GCM data has this happen at a 1 in 10 probability. (Of the 3 GCMs, one model tends to maintain the current flow, including the minimum flow, while the other models show a sharper reduction.) If instead we use the GCM model directly without downscaling to regional conditions, however, the effect of the climate change on flow reduction is far greater. What would now be considered extremely low flows (with a 1 in 1000 chance) can happen with a 1 in 10 chance (according to one of the climate models).

To determine the effect of the altered climate on the operation of the Hammond plant, a model of plant operations was developed. The variables downscaled from the GCM now include temperature, humidity, wind speed, and cloud cover, all of which determine the rate at which heat is removed from the river downstream from the plant discharge point. Early indications are that the plant may need to adapt to climate change, either by reducing power output, or through the construction of a cooling tower to dissipate heat.

Global climate model simulations have become a fundamental part of climate prediction, as only these models can encompass the global processes (jet streams, El Nino, stratospheric dynamics, etc.) that can affect regional climate. These cannot form the sole basis for a regional climate prediction, however, as the coarse grid spacing will necessarily miss the small-scale surface and atmospheric features that can lead to large meteorological differences between two relatively nearby locations. The application of a downscaling process can be used to bring GCM simulations of the 20th century in line with observations, and this correction can be applied to future GCM data for a more accurate prediction.

We used a simple, scaling downscaling method to get a prediction of temperature and precipitation data for the 2040s, then used this to get a prediction of the flow within the Coosa River basin upstream from the Plant Hammond for that period. We also created such a simulation with unscaled data taken from the original GCM simulations. The contrast between the two was clear – the use of downscaling led to significantly greater flows in the basin than the simulation does without downscaling, which called for strong decreases in the basin. A water management plan based on the latter would call for much more stringent restrictions than one based on the former. It is in this way that we feel the downscaling demonstrates its usefulness. An important caveat, however, is that the operation of the Hammond plant downstream of this basin may nevertheless face restrictions unless mitigating actions are taken.

FY 2011 Strategic Initiative Project Summaries

Nano-Photocatalysts for Solar Fuels Applications: Conversion of CO₂ to Hydrocarbons, S. Hunyadi Murph, K. Heroux, T. Sessions, R. Lascola, B. Peters, Y. Zhao (UGA), S. Ullrich (UGA), A. Greytak (USC), S. Retterer (ORNL)

We amassed a library of active nanohybrid catalysts with multifunctional, broadband electromagnetic response for solar energy conversion of CO₂ to fuel. The catalytic potential of the newly produced nanohybrid materials toward the photodegradation of a model analyte, methyl orange, was studied under UV and visible illumination. The photocatalytic performance of these nanomaterials was highly dependent upon nanoparticle shape, morphology, composition, crystallinity, and illumination. A solar cell solar-gas reactor for CO₂ conversion that allows evaluation and optimization of nanocatalysts for solar fuels applications was designed and built. Preliminary tests suggest production of hydrogen on titania based nanoparticles as depicted by residual gas analyzer (RGA) system.

The development of improved and efficient nano-photocatalysts for renewable fuel production from carbon dioxide (CO₂) and water has the potential to enable the long term, sustainable production of storable, transportable fuels. While this conversion can be achieved with the help of photocatalysts, the optical to chemical conversion efficiency has generally been very low, less than 0.5%. This is because most of the photocatalysts have a very narrow band edge absorbance, and provide limited amounts of free electrons and protons on the surface for such a reaction. The

overall goal of this proposal is the creation of actively controllable and tunable nano-photocatalysts with multifunctional, broadband electromagnetic response for solar energy conversion of CO₂ to fuel. Two interconnected directions of research are explored to enhance photocatalytic carbon dioxide conversion rates: (a) Development of innovative and tunable nanohybrid architectures with different topography, crystal structure, relative composition and interfacial area in a controllable manner for efficiently coupling light-harvesting, photo-redox processes, and photocatalytic behaviors; (b) Design and building of a solar cell solar-gas reactor for CO₂ conversion that allows evaluation and optimization of nanocatalysts for solar fuels applications.

Our efforts have been devoted to *production* (e.g. solution chemistries, glancing angle deposition (GLAD) and nanolithography) and *sensitizing TiO₂* with nanoparticles that absorb light at lower photon energies, extending absorption into the visible light region of the spectrum. This includes noble metals (NPs) (Au, Au-Pt, Ag, etc.), quantum dots (QDs) (CdS, CdSe, core-shell), and other oxides (WO₃, SiO₂, Fe₂O₃). Light absorption for these materials was tuned either by surface decoration of metal nano-islands, doping, core-shell design, or a combination of multi-bandgap nanocatalysts. Molecular self-assembly and co-deposition procedures have been employed to modify the TiO₂ surface. An assortment of parameters was investigated including the choice of bifunctional linker molecule, concentration, pH, temperature and solvent. We successfully produced tunable core-shell one-dimensional nano-architectures. This includes a variety of sizes, shapes and morphologies of Au- or Ag-TiO₂, -SiO₂/TiO₂, WO₃/TiO₂ and TiO₂/WO₃ photocatalysts. We have also prepared water-soluble nanomaterials (NPs and QDs) with various surface ligands, and we functionalized them onto TiO₂-based nanomaterials. QDs/TiO₂ sensitization via functionalization and oblique angle co-deposition approach was successfully achieved. This was done by systematically and gradually doping (from 0% to 100%) with QDs. Our work on rational decoration of TiO₂ substrates with metallic (Au) nanorods revealed limited success. Though this particular procedure requires optimization in order to achieve greater coverage of the array surface with metallic nanoparticles, good enhancements in photocatalytic activity were observed. Refinements of linking chemistry and substrate surface treatment to improve this process are under investigation. We have essayed a variety of techniques for characterization of these nanomaterials: SEM, TEM, UV-VIS, ellipsometry, photoluminescence, XRD, EDX, AFM, QCM, Raman, ξ potential, and reflectance spectroscopy. *Mathematical and theoretical calculations* (e.g DFT, Boltzmann equation, Tauc plots, Lambert-Beer's law) were also used to validate ongoing experimental work.

The *catalytic potential* of the newly produced nanohybrid materials toward the photodegradation of a model analyte, methyl orange, was studied in UV and visible illumination. The Langmuir-Hinshelwood model for pseudo-1st order degradation of organic pollutants was used to calculate degradation rates. We demonstrated that the catalytic performance of these nanomaterials is highly dependent upon the nanoparticles' shape, morphology, composition, crystallinity, and illumination condition. Among the samples tested, core-shell nanomaterials show the best catalytic activity, when compared to pure TiO₂ arrays of the same shape. We determined that by annealing TiO₂ at temperatures above 200°C, the crystal structure changes from amorphous to anatase and the number of defect sites is reduced, thus improving photocatalytic efficiency. Shape-dependence of the nanomaterials on catalytic activity was exhibited in both visible and UV light with the diamonds showing greater reactivity than their triangular or spherical counterparts. This is likely due to the

presence of more edges and corners in the diamond/triangle array which tend to be more reactive, as well as different crystallographic facets. In the visible region, the photocatalytic activity of Au rods/TiO₂ is also improved when compared with bare TiO₂ arrays (shows no MO degradation in visible light) despite suboptimal coverage of the TiO₂ pillars. This clearly indicates that AuNRs play an essential role in sensitizing TiO₂ to visible light. The photocatalytic decay rates for Fe₂O₃ samples were highly dependent on the morphology of the sample, as follows OAD>GLAD>TF.

A *photocatalytic reactor test* system consisting of a home-designed chamber (with gas inlet and outlet, optical window, sample stage holder, heater and temperature sensor), pump system (rotary pump and turbo pump) and either a residual gas analyzer (RGA) or gas chromatograph was built and is ready for use (Figure 1). Preliminary data generated after several hours' exposure in saturated CO₂, on TiO₂-

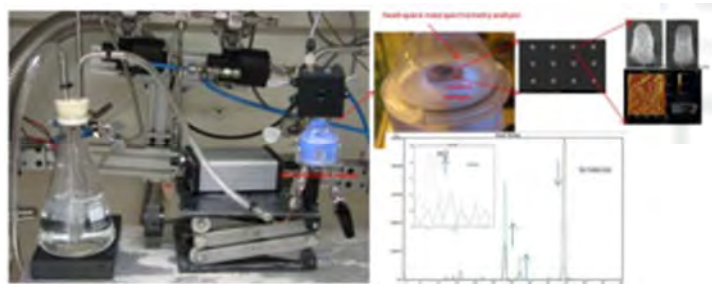


Figure.1. Photo-catalytic reactor system (left), SEM /AFM images of Au- QD- TiO₂ nano-photocatalyst (top), RGA data showing H₂ production (bottom).

based photocatalysts under UV exposure, suggests generation of hydrogen gas. While some hydrocarbons may also be produced clear identification/validation of these products was difficult due to problems encountered with gas/air in/out flow (leakage). However, it is anticipated that once the leakage is completely resolved, routine analysis will be performed with the reactor on optimized nano-photocatalysts. A *home designed spectrophotometer coupled with fluorescence* capabilities has been built in house for routine UV-Vis absorption spectroscopy, transmission and reflectance measurements, as well as fluorescence/ phosphorescence analysis. We are also adapting an existing *DC&RF sputter deposition system* currently at SRNL to potentially produce ordered arrays of nano-catalysts of interest. We demonstrate the viability of this technique by producing ordered arrays of Ag nanostructures. An *ultrafast transient absorption system* was also built at UGA to provide essential information on the mechanistic and kinetic details of chemical events that occur in the timescale of 10 femtoseconds to 100 picoseconds. Optimization experiments are underway to achieve higher resolution measurements. *In conclusion*, we amassed a library of active nanohybrid catalysts for photodegradation of organic dyes in the visible and UV region. Preliminary tests show production of hydrogen gas on TiO₂-based catalysts and possibly other hydrocarbons after several hours' exposure in saturated CO₂ medium. We designed and built several new instruments that expand SRNL's capabilities and competencies.

Reactive Gas Recycling of Used Nuclear Fuels, J. Gray, P. Korinko, M. Martinez-Rodriguez, S. Sherman, R. Torres, B. Garcia-Diaz, G. Morgan, A. Visser, T. Sudarshan, and T. Adams

Nuclear Energy will be a key element in the development of a long long-term, clean sustainable energy solution in the Unites States. Development of advanced, economical Used Nuclear Fuel (UNF) recycling

technologies to close the fuel cycle is an important facet of this solution. Recycling of UNF is a complex problem that poses both technical and non-proliferation policy challenges. Widespread implementation of commercial UNF recycling necessitates the development of low-cost, safe, reduced-footprint technologies that are inherently proliferation-resistant. In an effort to develop an innovative breakthrough to facilitate a widespread renaissance of nuclear energy technologies, SRNL has been at the forefront of the movement to develop novel dry reactive gas recycling (RGR) technologies for UNF. These dry technologies have the potential benefit of generating significantly reduced levels of liquid waste in a modular low-cost design with an inherently simplified process flow sheet and a reduced process footprint. Current SRNL research efforts indicate the possibility of developing both closed and modified-open recycling schemes based on dry process operations. The reported research is comprised of theoretical analyses and experimental characterization to advance the development of a novel dry recycling concept for used nuclear fuels. This program will develop the scientific basis for candidate dry waste processing routes to cover full cradle-to-grave recycling and will provide the fundamental scientific knowledge that will allow us to find an optimal separations process for low-cost fuel recycling, liquid waste reduction, and proliferation resistance.

The research reported has the overarching objective of putting SRNL into a technical and business leadership position in the development of alternate UNF recycle processes. SRNL is proposing an all dry recycling technology based on simultaneously reacting UNF materials with a mixed-gas environment as an alternative to current aqueous technologies. This research would leverage SRNL leadership in aqueous processing and adapt it to investigate emerging dry recycle technologies. This dry process can be designed to efficiently separate the actinides in proliferation-resistant schemes while at the same time making these valuable resources available for recycle/reuse in commercial or advanced burner reactor fuels. The development of dry separations and recycle technologies is a transformational technology for the advancement of next generation nuclear energy production.

The reported work consists of two main thrusts which extend to the particular approaches to dry recycle technology development – theoretical analysis and experimental data collection. The first aspect of the research consists of development of more rigorous theoretical calculation tools comprising thermodynamic prediction and reaction pathway and kinetic analysis. The second key area involves development of experimental reactors and analytical measurements to test hypotheses and process conditions for the targeted approaches to dry UNF recycle. These two thrusts will be used to develop a flowsheet modeling tool to assist in the development of a representative framework for dry UNF recycle technologies developed at SRNL.

A significant amount of progress has been accomplished in each of the areas investigated for the development of the RGR technologies for UNF. Preliminary calculations have been conducted which point to the potential efficacy of using XeF_2 as an alternate fluorinating agent for separation of key UNF species, and a milligram-scale reactor has been constructed to test this separation. This reactor has been benchmarked and is in the process of being optimized to promote reaction of the solid UNF materials with the reactive gas streams. Additionally, a larger scale reactor has been constructed and will be benchmarked in the coming fiscal year which can be used for multiple purposes. This reactor can potentially hold gram-scale quantities of solid reactants and thus can

Risk Reduction and Process Optimization for Engineered Algae Production

Systems, Michael Heitkamp, C. Bagwell, C. Yeager, S. Sherman, C. Berry, C. Milliken, T. Soule, K. Sander, R. Barrier, M. Piskorski(USCA), P. Moeller(NOAA), P. Zimba (Texas A&M)

SRNL established fundamental algae growth capabilities that significantly increased core capabilities in algae bioprocess development. The new growth systems include both bench- and floor-scale systems designed to provide automated control of key variables such as gas delivery, temperature, light intensity, light cycle, pH, CO₂, nutrient input, liquid recycling and data logging. Three bench-top photobioreactors are Biostat PBR 2S units manufactured by Sartorius Stedim (Germany). The floor-scale unit is a MPP-30 algae photobioreactor manufactured by Lab Glass Apparatus that was extensively modified and automated by SRNL. All eHAPs, building facility modifications, system modifications, safety inspections and startups are complete. These growth systems provide unique capability for algal bioprocess development relevant to process risk assessment and bioprocess optimization. Moving forward, SRNL will utilize various biofuel production strains to evaluate the impacts of different inorganic contaminants (RCRA metals), typical to wastewaters and flue gas, on growth and productivity, as well as potential for inducing production of bioactive compounds (toxins) and volatile organic compounds (VOCs).

This project consists of four overall objectives: 1) Design, procure, construct and start-up algae R&D growth platforms. These systems provide new capability for fundamental work to characterize and optimize algae growth and performance; 2) Evaluate the occurrence, partitioning and impacts of different key inorganic components from municipal and industrial wastewaters and flue gases on algae growth and performance; 3) Screen several selected algal cultures and production strains for production of bioactive compounds and investigate the impacts of metals and contaminants on toxicity profiles; and 4) Conduct initial scoping calculations and flow sheeting for algae production systems accounting for any contaminant impacts on process design. Since large scale production of algae has significant requirements for water, nutrients and CO₂, there is growing interest for integration of algal systems with both wastewater and flue gas CO₂ sources. This scaling-up of algae production, and the cross-market integration of products and co-products to animal feeds, have recently raised major concerns for bioprocess performance, quality assurance and safety. Concentrating on risk reduction and process optimization is a natural fit for SRNL, provides differentiation from other players in the algae area and provides fundamental algae capability that will enable growth of new business and establish SRNL leadership in a rapidly emerging clean energy sector.

The bench- and floor-scale algae growth systems were designed to provide automated control of key variables such as gas delivery, temperature, light intensity, light cycle, pH, CO₂, nutrient input, liquid recycling and data logging. Three bench-top photo bioreactors are 3-liter Biostat PBR 2S units manufactured by Sartorius Stedim (Germany). The floor-scale unit is a MPP-30 algae bubble column photobioreactor manufactured by Lab Glass Apparatus (5, 10 L glass columns) and was automated by SRNL to provide process control through LabView for real-time data collection. Work was also conducted to isolate, screen and culture natural freshwater algae strains that grow well in the region and are good oil producers.

All eHAPs, system modifications, safety inspections and startups are complete for the bench- and floor-scale algae growth systems. All process monitoring and control apparatus are installed and functioning successfully with LabView software. More than 100 environmental samples have been screened for natural algal strains that grow well in the Southeast and more than 50 unialgal strains have been isolated. Currently, 10 different *Chlorella* strains from our collection are being utilized for grow-out studies in the floor-scale bubble column photo bioreactor. An interagency agreement with NOAA and a subcontract with Texas A&M were successfully placed to enable toxin screening and VOC analyses, respectively. Both NOAA and Texas A&M collaborators have recently begun to receive algal samples from SRNL for evaluation. Moving forward, SRNL will utilize recently isolated algae strains to evaluate the impacts of different inorganic contaminants (RCRA metals) typical to wastewaters and flue gas on growth and productivity, as well as production of bioactive compounds (toxins).

SRNL has significantly increased capabilities for large scale growth of algae, bioprocess development, process optimization and risk assessment. Integrated modification of these systems provides fundamental capability for controlled growth of algae under a variety of experimental conditions. The isolation of native algae strains was completed, and are currently being used in grow-out experiments. Key partnerships are now in place providing capability to screen algal samples for bioactive compounds and volatile organic compounds. In early FY 2012, SRNL will purchase a continuous flow centrifuge to provide capability to efficiently harvest and concentrate algae from the grow-out systems. Moving forward, SRNL will examine the impacts of nickel and copper on growth, lipid production, and toxicity in several algae strains.

FY 2011 Standard Project Summaries

Advanced Gas Sensors Using SERS-Activated Waveguides, R. Lascola, S. Murph, J. Reppert, K. Heroux, S. McWhorter

This work is directed towards the development and implementation of gas detection methodologies based on Raman spectroscopy. Our goal is to provide a lower-cost, in situ alternative to mass spectrometry techniques currently employed at the Tritium production facilities at SRS. Raman spectroscopy is attractive for IR-inactive molecules (e.g. H₂ and its isotopologues) or scenarios where infrared technology is inconvenient. Previous work by our group demonstrated detection limits of 6-7 Torr for H₂. We have improved the detection limit through the use of multipass optics, metallic waveguides, and waveguides coated with nanoparticles that generate surface-enhanced Raman scattering (SERS). We have observed 25x signal enhancement with Ag-coated capillaries with no nanoparticles. We have seen an additional 2-5x enhancement with the addition of nanoparticles, despite suboptimal surface coverage. This is a novel implementation of the SERS technique that shows great promise for measurements of process gases.

The intent of this research is the development of a practical device for measuring low concentrations of gas-phase analytes by Raman spectroscopy. The first phase of the work is the development of reflective waveguides (glass tubes that have been coated on the interior with gold or silver) that serve as gas cells. Compared to conventional configurations, the waveguides allow for a greater sampling volume and more efficient collection of Raman scattering. Sensitivity improvements of 15-30x are reported in the literature, which if replicated would be useful for analysis in the SRS Tritium process and elsewhere. The second phase is further improvement of detection limits through the development of waveguides that exhibit surface-enhanced Raman scattering (SERS). SERS, despite being known in the research environment for several decades, has not yet been widely implemented in a practical device, nor has it been used in a general technique to enhance the detection limits of Raman spectroscopy for gaseous analytes. Incorporating SERS-active particles into a waveguide increases the interaction area of the exciting laser and the analyte, potentially improving the sensitivity and consistency of the SERS response. An additional order of magnitude of sensitivity could be realized over conventional waveguides, bringing detection levels to the low part per million levels. Such sensors would have applications to weapons monitoring, process analysis, and field analysis of trace vapors.

The first step was to develop a reliable technique for making Ag-coated waveguides (Ag being determined to have the highest reflectivity for the laser wavelength being used). We accomplished this through deposition from a colloidal Ag solution, after appropriate glass cleaning. Next, we determined the optical performance of the waveguides by Raman measurements of N₂ and O₂ from air, or H₂/HD/D₂ or CO₂/CH₄/N₂ mixes. We constructed a protective flow cell into which we could couple the laser, introduce gases, and sample the Raman scattering. Finally, we investigated the chemistry required to attach Au nanoparticles (rods of dimension 25 x 60 nm) to the Ag surface. Important parameters considered here include the choice of linker molecule (dithiol v. aminothiols, chain length), solvent system, and reaction time. In addition to characterization of the Raman response, the surfaces were imaged by scanning electron microscopy (SEM) to determine surface coverage of the nanoparticles.

The development and characterization of the Ag waveguide was successful. We adapted a commercial gilding process to make up to 8 reproducible waveguides in half a day. Using a forward-scattering geometry to optimize collection efficiency, we observed the best waveguide length to be approximately 25 cm, with a linear dependence of signal on diameter to at least 3.2 mm. We observed a 25x improvement in Raman signal compared to previous work using conventional configurations. This translates to absolute detection limits of about 0.1 Torr for H₂ and less than 0.5 Torr for N₂, O₂, and CH₄.

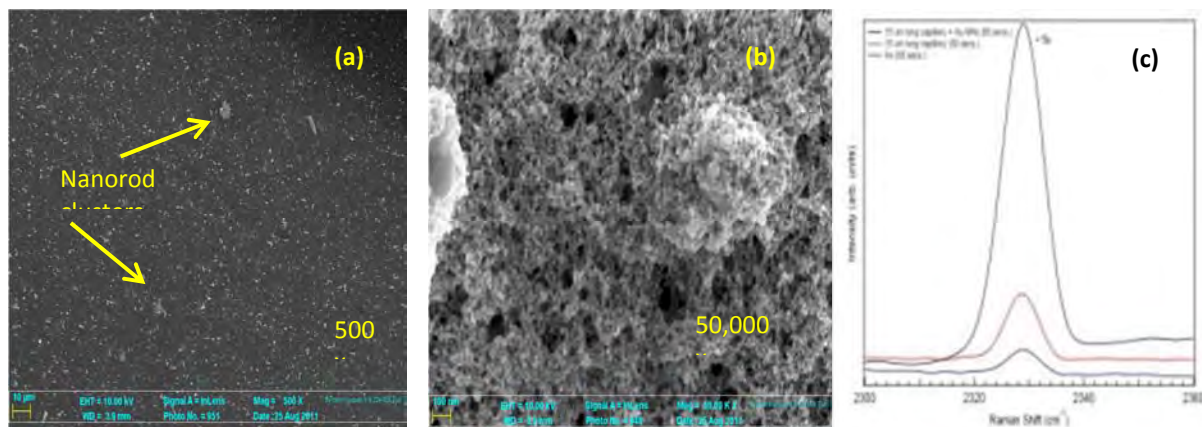


Figure 1. (a) SEM image of a functionalized waveguide interior. Clusters of Au nanorods are indicated. (b) Detail of nanorod cluster. (c) Raman spectra of N₂ in air (bottom), in Ag waveguide (middle), and in functionalized waveguide (top).

Although development of the SERS-active waveguide is incomplete, we obtained promising results. The primary problem we encountered was difficulty in obtaining widespread coverage of the surface with the Au nanorods (Figure 1a). The nanorods exhibit a stronger attraction to each other than the Ag surface (Figure 1b). We observed mild improvements when using alcohol-based solvents for the nanorods, when using dithiol versus aminothiols linkers, and when using longer-chain linker molecules. We also observed better nanoparticle coverage at the ends of the waveguides rather than the center. Despite these problems, the nanoparticle-enhanced waveguides did show more Raman scattering than plain Ag waveguides (Figure 1c). Enhancements for N₂ were 1.5-3x for 10 cm waveguides and 5x for 15 cm waveguides. Light transmission is actually slightly *lower* for these waveguides, indicating that the increased signal is not due to enhanced reflectivity.

In conclusion, we have demonstrated 25x greater sensitivity to gases with Raman spectroscopy using Ag waveguides. That alone is a significant expansion of SRNL capabilities, and additional work is planned to test the waveguides for use in SRS facilities. We have also observed further signal enhancements with nanoparticle-functionalized waveguides under conditions that suggest that enhancement is due to the SERS effect, despite suboptimal coverage of the waveguide surface.

We acknowledge the valuable advice and laboratory work of Dr. William Spencer, Dr. Patrick O'Rourke, and Mr. Brent Peters of SRNL, and Prof. Michael Angel of the University of South Carolina-Columbia.

Application of Cooling Towers for Collection, Concentration, and Detection of Biological Agents, and Elemental Chemicals, R. L. Brigmon, M. T. Kingsley, W. L. Jones, S. Leskinen (University of South Florida), E. Kearns (University of South Florida) & D. Lim (University of South Florida)

This project demonstrated that cooling towers could serve as collection platforms for airborne particulate biological targets. This project also confirmed that further concentration of particulates entrained in the cooling tower water, as well as inorganic metals, was possible using the Portable Multi-use Automatic Concentration System (PMACS). Bacillus thuringiensis israelensis (Bti) spores sprayed near an SRS tower were detected in cooling tower water within 15 minutes and remained detectable for 3 days. Concentrations of target microorganisms Legionella pneumophila (Lp) and Bti collected using 500 ml grab samples and 100 L PMACS samples demonstrated Lp concentrations below current detection limits. Concentration of cooling tower water enhanced inductively coupled plasma-mass spectrometry (ICP-MS) detection of isotopes of cobalt, rubidium, molybdenum, barium, lanthanum, cesium and lead. Test results suggest that the cooling tower + PMACS approach will enable exploitation of widely dispersed existing cooling towers as biological, and potentially, chemical and radiological environmental monitoring systems.

Current detection and/or tracking methods for bioterrorism threats on an urban scale are extremely limited. The objective of this project was to demonstrate that cooling towers can be exploited to greatly improve air monitoring for biological agents of concern. The capacity of cooling towers to collect or entrain compounds from air (1000's ft³/min, 24/7) exceeds that of current air monitoring technologies. Cooling towers are ubiquitous in industrial, municipal, and military environments, including many overseas locations, and could prove useful in thwarting such events. The significance of this approach is the exploitation of existing infrastructure (cooling towers) to serve as environmental collectors to augment traditional environmental monitoring systems, such as BioWatch. Knowledge of specific tower operations, e.g water turnover & blowdown, can be used to optimize sampling. In addition, cooling tower water can be further concentrated quickly and easily using a technology developed at the University of South Florida (USF). The Portable Multiuse Automated Concentration System can collect particulates in very large volumes of water (tens to hundreds of liters) and recover them in a much smaller volume of liquid (< 500 ml). The concentrated liquid samples can be then be analyzed by any method desired. The proposed approach is based upon two existing technologies (cooling water towers and PMACS) that allow for broad range particle collection/concentration and could be used to facilitate detection of radiological and chemical, as well as biological, targets of interest in air following their entrainment in the tower water.

Several well characterized cooling towers were selected for evaluation of PMACS enhancement of the SRS *L. pneumophila* surveillance program. A total of thirty four 100 L samples and sixty-two 500 ml grab samples were collected between August 2010 and May 2011. Grab samples were taken prior to and immediately after PMACS samples. Water from two tower basins was sampled in August to assess the most appropriate direct fluorescent antibody (DFA) and polymerase chain reaction (PCR) protocol for the PMACS retentates.



Figure 1. Clockwise from upper left: Anderson impactor sampler (viable cultures), two photos of RADeCO air filter sampler (Model H-180), Dyna-Fog Hurricane™ (Model 279) Sprayer (PCR and DFA testing) and Bti aerosol spraying towards cooling tower 285-F, Anderson impactor, technician programming filter sampler, cooling tower 285-F and visible aerosol Bti-containing mist exiting Dyna-Fog sprayer.

Due to the variety of tower types at SRS, those tower basins were sampled again in September together with an additional three towers to evaluate the general applicability of the PMACS to a *Legionella* surveillance program. F-Area Cooling Tower 285-11F was sampled exclusively to provide statistical validation of the PMACS' performance for *Legionella* detection. In parallel with the *Lp* testing, one spike and three aerosol spray tests using *Bti* were conducted with F-Area Cooling Tower 285-11F in February, March, April and May, 2011. The PMACS concentrated 100 L of water and compared to 500 ml "grab" samples.

Figure 1 shows results a representative experimental set up for *Bti* aerosolization and monitoring in March, 2011 testing where before spraying *Bti* was below detection. *Bti* was detected (10^8 cell/L) in the tower water within 1 hour of aerosol application, indicating *Bti* entrainment in the water. The *Bti* persisted for up to 3 days after spraying. All samples were tested with *Bti*-specific DFA, PCR, and culture techniques. These results indicate that cooling towers could be used in biosurveillance for agents such as *Bacillus anthracis* (anthrax) that could be disseminated through aerosol release. *Lp* was detected consistently with the concentrated 100L retentate where in certain comparative 500 ml samples tested negative for *Lp*. Collection of *Bti* and *Lp* from ambient air showed release of these agents from the cooling tower.

Radionuclides and many chemical agents are strongly associated with particles. In the April 19, 2011 test samples collected from the basin of F-Area cooling tower 285-11F, using either PMACS concentration or a standard "grab" collection of 500 ml were analyzed by inductively coupled mass spectrometry (ICPMS). The ICPMS results demonstrated that isotopes of cobalt, rubidium, molybdenum, barium, lanthanum, cesium, and lead were below detection in the unconcentrated cooling tower water but detectable in the PMACS retentate. Cesium 133 was detectable in both samples but the concentration was increased by the PMACS. These data strongly suggest that the detection of chemical compounds in cooling tower water is a means of monitoring agents of concern.

Current detection and/or tracking methods on an urban scale are extremely limited. Knowledge of specific tower operations, e.g water turnover & blowdown, can be used to optimize sampling. Therefore, demonstrating that these can be exploited to greatly improve air monitoring for a dispersed, wide area monitoring system for a spectrum of targets and applications was the point of this project. The capacity of cooling towers to collect or entrain compounds from air (1000's cubic feet per minute 24/7) is expected to exceed that of current air collection technologies. One benefit

of the proposed approach is that the devices needed (cooling water towers and PMACS) are existing technologies and can allow for broad-spectrum collection/concentration method to facilitate detection of radiological, chemical and biological targets of interest in air – they become entrained in the water. The concentrated liquid samples can be then be analyzed by any method desired by the investigator.

Can Ionic Liquids be used as Templating Agents for Controlled Design of U-Containing Nanomaterials?, A. Visser, N. Bridges, and A. Duncan

Nanostructured oxides have been prepared in ionic liquids (ILs) using different ILs as templating agents. Using ILs as reaction media for inorganic nanomaterials takes advantage of the pre-organized structure of the ILs to template inorganic nanomaterials. In this project, ILs were used in low temperature synthesis of uranium oxides. The variation of IL cation structure was investigated to determine the impact on the metal oxide morphologies. For a selected IL cation, increasing the alkyl chain length increases the aspect ratio of the resulting oxides.

Understanding how the resulting metal oxide morphologies impact fuel pellet properties could enhance fuel stability and design. A U-containing oxide was used in fuel pellet fabrication and subsequent pellet testing.

Metal oxide synthesis experiments were performed using a low temperature route. Uranyl acetate was combined with either NH_4OH or NaOH and the selected ionic liquid and heated to $150\text{ }^\circ\text{C}$ for 48 hours. The product was rinsed with water and isopropanol and then characterized.

XRD analysis of the products revealed the syntheses produced a mixture of sodium uranium salts or ammonium uranium salts. However, TEM analysis identified UO_2 and U_3O_8 as well as amorphous solids. Product morphologies were determined using both SEM and TEM, with their elemental composition determined using electron dispersive spectroscopic analysis. Figure 1 shows TEM images and electron diffraction patterns of products from synthesis with 1-dodecyl-3-methylimidazolium tetrafluoroborate ($[\text{C}_{12}\text{mim}][\text{BF}_4]$, top) and 1-octyl-3-methylimidazolium tetrafluoroborate ($[\text{C}_8\text{mim}][\text{BF}_4]$, middle).

The TEM image of one of the $[\text{C}_{12}\text{mim}][\text{BF}_4]$ products is shown in Figure 1 part A. Elemental analysis shows the rods contain U, C, and O. The rods are amorphous and show no spots in the electron diffraction pattern (A2). The TEM image in Figure 1 part B is the other product from the $[\text{C}_{12}\text{mim}][\text{BF}_4]$ synthesis. The electron diffraction pattern (B2) reveals the solid to be cubic UO_2 .

The TEM image of the products from $[\text{C}_8\text{mim}][\text{BF}_4]$ synthesis are shown in Figure 1 parts C and D. Nanoparticles in part C contain U, C, and O. Electron diffraction of these solids (D2) suggest they are U_3O_8 . The $[\text{C}_8\text{mim}][\text{BF}_4]$ synthesis product also contained nanostars composed of UO_2 (part D).

Using the IL synthesis, U-containing materials were prepared for pellet pressing and sintering. The samples were pressed in a stainless steel punch and die tool. Approximately 330MPa of pressure

were exerted on the tool. The pellets were removed from the tool and then sintered at 1100 °C for 100 mins. The resulting pellets were characterized.

The uranium oxide in Figure 1 (bottom) is from the synthesis with $[C_4mim][BF_4]$. The dimensions were measured before and after sintering. The control samples compacted under pressure in a well behaved manner, but those synthesized with ILs extruded through the annular space between the anvils and the cylinder of the die. To accommodate this, the pellets synthesized from ILs were pressed at lower pressures closer to 50 MPa. The pellets were removed from the die and transferred to a tube furnace for sintering at 1100 °C for 100 minutes in flowing argon. The resulting pellets were characterized to determine the amount of densification that occurred during sintering. The control samples reacted with the furnace tube and were not recovered. The samples made with ILs were recovered. The IL samples experienced volume reduction ranging from 20 to 31.5% reduction which was expected for this sintering temperature.

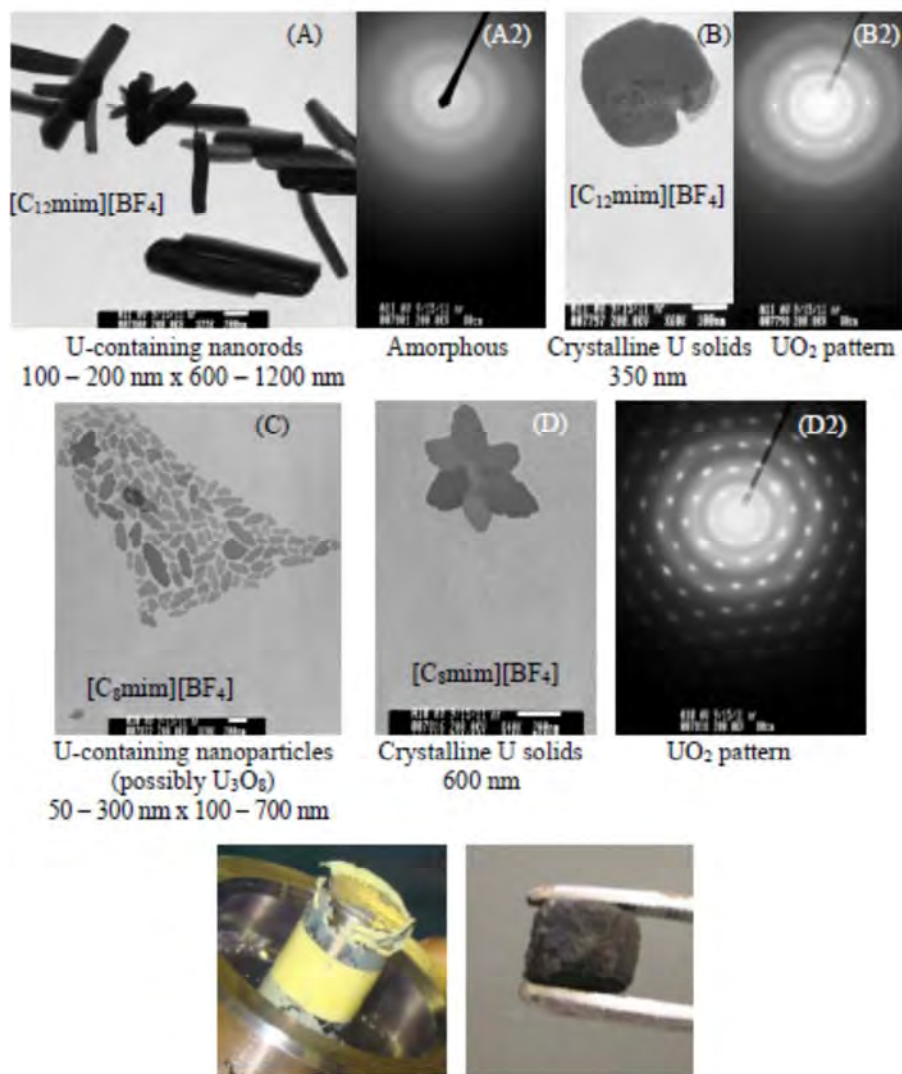


Figure 1: Uranium oxide morphologies (top, middle) and pellets (bottom, left = pressed pellet, right = sintered pellet)

These initial results show the utility of ILs as a novel route for actinide oxide preparation. Further work to optimize the synthesis parameters and pressing conditions is warranted. The data from this LDRD will be used as the basis for developing a fundamental understanding of the properties of the oxides produced in this fashion. This fundamental understanding will enhance the scientific basis necessary for furthering the field of ILs for advanced spent fuel fabrication technologies and guide future investigations of these novel chemical materials for nuclear energy applications.

Carbon Nanomaterials with Encapsulated Gadolinium for Advanced Neutron Detection, *S.L. Garrison, L. C. Teague, J. R. Coleman, T. B. Brown, M.R. Kriz*

We designed, fabricated and tested a prototype solid-state neutron detector based on gadolinium, which was encapsulated in a carbon-based nanomaterial. Initial, proof-of-concept experiments confirmed that conversion electrons produced by the encapsulated gadolinium could be detected in a liquid scintillation style design. Although the thin-films for the solid-state design were electrically conductive, there was no measurable response or difference in their electronic properties under neutron irradiation. As such the thin-film design was deemed unsuccessful.

Helium-3 (He-3) is commonly used for neutron detection, especially for purposes related to the prevention of nuclear terrorism. As a major source of He-3 is from the decay of tritium, which has seen a near-complete reduction in its production within the US, the supply of He-3 is rapidly dwindling, to the point of a shortage. A replacement neutron detector technology is required, and in many cases this new technology must also be able to discriminate between neutrons and gamma-rays. However, current alternatives tend to require low temps (O(100 K)) or hazardous materials (e.g., BF₃) or they do not provide gamma-ray (γ -ray) discrimination. Gadolinium-157 (Gd-157) provides a high cross-section for thermal neutron absorption for excellent sensitivity and a solid-state, thin-film detector design could provide discrimination from background γ -rays by limiting the time an incident γ -ray can interact with the Gd. The goal of this work was to design, fabricate, and test a prototype solid-state neutron detector based on gadolinium because of its high cross-section for thermal neutron absorption.

In Phase I, we mixed a commercial, off-the-shelf gadolinium-encapsulated, carbon-based nanomaterial (Gd-ECBN) with an organic scintillator dissolved in o-xylene. Upon absorption of a neutron by the gadolinium (Gd) within the Gd-ECBN, one or more a conversion electrons would be produced by the Gd that would be converted into light pulses by the scintillator for detection via a standard photomultiplier tube (PMT) setup. Control solutions of (1) the scintillator and of (2) the scintillator with a carbon-based nanomaterial (C70-PCBEH) similar to the Gd-ECBN (but without Gd) in o-xylene were also made. These solutions were irradiated with a ²⁵²Californium (²⁵²Cf) source in the Low Scatter Irradiator (LSI) at the Savannah River Site's Health Physics Instrument Calibration Facility (HPICL). The goal of Phase I was to provide basic proof-of-concept confirmation that conversion electrons produced by the Gd could be transferred to the rest of the carbon nanomaterial (and beyond) for detection. In Phase II, we mixed the Gd-ECBN, at its maximum solubility, with a commercially available, conductive polymer (polyaniline (PANI)) dispersed in o-

xylene. Thin-films of PANI, PANI+C70-PCBEH, and PANI+Gd-ECBN were deposited as thin films upon gold electrodes atop a silicon substrate via spin-coating. Electrical testing, namely measurements of steady state currents and IV curves, confirmed that the films were conductive and set the baseline for measurements without neutron irradiation. Steady-state currents for these films were measured at an applied voltage of 1V immediately before, during, and immediately after exposure to the aforementioned ^{252}Cf source in an attempt to detect a measurable electrical signal.

For the Phase I experiments, approximately 7ml of two different concentrations were used for the Gd-ECBN solutions: 1 wt.% and 0.01 wt.% Gd-ECBN. The C70-PCBEH solutions were such that the molar concentration of the C70-PCBEH nanomaterial were equivalent to the molar concentration of the Gd-ECBN in its solutions. The 1 wt.%-equivalent solutions were quite black, and the scintillation results indicated that they absorbed nearly all of the photons generated by the scintillator. For the control solution of just scintillator and o-xylene, the Hidex unexpectedly reported 2-3 million counts (photons detected) per minute. This was significantly more than the 1.6 to 1.8 million counts per minute (CPM) for the C70-PCBEH and Gd-ECBN. It is possible that the Gd-ECBN solutions were absorbing some of the photons produced upon neutron absorption by the Gd as the solutions were transparent, but not 100% clear. We also believe the glass vials containing the solutions may have been borosilicate glass such that the significant response was due to neutron absorption by boron, which has an isotope with high neutron cross-section, within the glass and the resulting ~ 0.5 MeV gamma photon released approximately 94% of the time it absorbs a neutron. Similarly-shaped soda-lime glass vials were obtained and the Phase I experiments were rerun with the 0.01 wt.%-equivalent solutions. While the Gd-ECBN solutions were more responsive to neutrons than the C70-PCBEH solutions ($1.87\text{E}6 \pm 1.2\text{E}3$ CPM versus $1.67\text{E}6 \pm 3\text{E}3$ CPM, respectively), these were still less than for the control solution with only o-xylene and scintillator. Given that the counts were similar to the original Phase I experiments, it seems plausible that there was still boron in the soda-lime glass. For Phase II, upon exposure to neutrons, the electrically conductive films showed no measurable electrical response compared to before or after neutron exposure. As such, the prototype designs for Phase II were deemed unsuccessful.

In conclusion, Phase I was a partial success in that sensitivity to neutrons by the Gd-ECBN material was demonstrated. However, the baseline signal, even in soda-lime glass, was significantly higher than for the Gd-ECBN solutions. Phase II was partial success in that thin films of PANI, PANI+C70-PCBEH, and PANI+Gd-ECBN were successfully generated via spin-coating and they were electrically conductive films. However, no measurable response or differences in their electronic properties were detected under neutron irradiation. As such, the prototype designs for Phase II were deemed unsuccessful. A patent disclosure based on an alternate methodology developed during this work is being submitted.

Charge Transport and Storage in Organic Semiconducting Materials: Toward Improved and Future Device Structures, L. C. Teague

The goal of the work described herein was to further the understanding of charge transport and charge trapping/storage phenomena in organic semiconducting materials used in organic-based device technologies such as organic-based transistors (OTFTs), organic-based memory, energy storage materials, organic light-emitting diodes (OLEDs), organic-based photovoltaics (OPVs) and organic-based radiation detectors. Specifically, this work addresses how charge trapping and storage in organic-based devices is influenced by the environmental conditions during operation. Organic-based materials are becoming increasingly popular due to their potential for high-performance, low-power, low-cost alternatives to existing technologies, however, the ability to control the charge transport and charge trapping in organic-based devices is a multifaceted challenge that is crucial to the development and sustainability of organic-based technologies.

The overall goal of these studies was to investigate how environmental conditions can affect the rate of charge accumulation and dissipation in organic thin film transistors (OTFTs). Specifically, these studies were aimed at understanding how charge is stored in these materials, how it can be manipulated, and if it can be trapped and released on demand. The charge trapping phenomena demonstrated by previous studies by the PI and others in the research community can be interpreted as having a deleterious effect on device performance, while at the same time, showing the positive potential of these materials for charge/energy storage applications. The discovery of methods to both reduce charging in organic-based devices as well as discovering ways to promote charge trapping and control charge dissipation will allow for future applications of organic thin film materials.

This work included the preparation and subsequent electrical and scanning Kelvin probe microscopy (SKPM) analysis of OTFTs. The electrical properties, nanoscale structural properties, and performance of these devices were evaluated under variable environmental conditions. The organic semiconductor used for these devices was synthesized for SRNL by Dr. John Anthony's research group at the University of Kentucky. Photolithography of sample test structures was accomplished at the CNM clean room fabrication facilities at Argonne National Lab (CNM user proposal #23377; use of CNM was supported by the U.S. DOE, Office of Science, BES Division, under Contract No. DE-AC02-06CH11357). Final OTFT device preparation and analysis was accomplished at SRNL. SRNL researchers also designed and fabricated a specialized testing platform to provide for electrical connections to the OTFT samples studied. This platform allows remote device operation and electrical testing while simultaneously collecting SKPM images of the devices.

Steady-state electrical measurements showed degradation in the OTFT performance (decrease in source/drain current) over time. SKPM images of the OTFTs reveal that this time-dependent degradation is due to trapped charge in the thin film that builds up during bias stress (application of the gate voltage) as shown in Figure 1. The degree of degradation was found to depend on a number of environmental factors. However, the SRNL project PI was able to develop a method to manipulate the charge transport in a way that can prevent this type of degradation in the performance of organic semiconductor-based devices. An invention disclosure that details this method has been submitted and a patent application is in preparation.

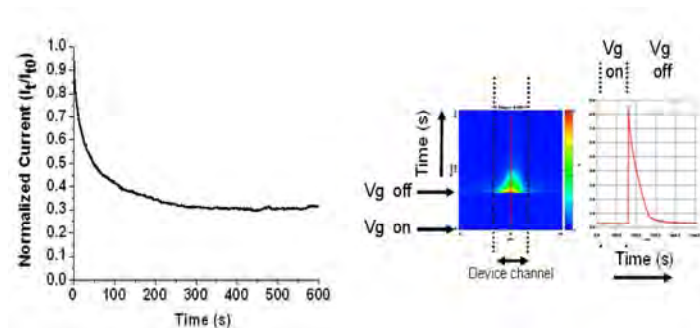


Figure 1. Steady-state response of an OTFT device (left). Constant bias $V_g = -40V$ and $V_{sd} = -20V$ are applied throughout and current is measured. Over time, the current (performance) decreases. SKPM image and corresponding line profile (right) showing charge stored during stressing of OTFT device for 150s with $V_g = -40V$. Dissipation of charge is observed over time following removal of V_g .

The experimental results will be submitted for publication in a peer-reviewed journal following submission of the patent application. The studies described herein and the results from these studies open the door for new technologies and applications in the area of organic-based electronics.

Engineering support from the following SRNL colleagues is gratefully acknowledged: R. Lascola, K. Huffman, J. DeGange, M. Hudson, B. Blackmon, and J. Jones

Detoxification of Uranium in Soils and Groundwater Using Recycled Concrete, M. Denham, B. Jones, A. Knox, and M. Whiteside

We conducted experiments to test the potential for recycled concrete to sequester uranium in contaminated soils and groundwater. Semi-quantitative experiments in which a small amount of various formulations of hydrated Portland cement and silica fume were mixed with solutions containing 1 mg/L uranium indicate >37% uranium removal by the cement amendments. There was a direct correlation between the percentage of Portland cement in a formulation and the amount of uranium removed. Likewise, the cement amendments reduced bioavailability of uranium in contaminated soils. In addition, we tested diffusive gradient in thin-films (DGT) probes for their ability to measure bioavailability of contaminant uranium in soils relative to extraction procedures. We conclude that the DGT probes are a better method for measuring bioavailability than the more aggressive extraction procedures.

The two technical objectives of this project were to test:

1. whether recycled concrete would be useful as an additive to soil and groundwater to reduce bioavailability of contaminant uranium

2. to examine the use of diffusive gradient in thin-film (DGT) probes to measure bioavailability of uranium and other metals in soils

Uranium is the most frequently occurring radionuclide contaminant in soil and groundwater of the DOE complex, but current treatment options are either reversible or apply to only a limited set of conditions. We propose that uranium(VI) can be immobilized by inducing precipitation of uranium(VI) silicates by addition of powdered recycled concrete. Uranium silicates, such as soddyite $[(\text{UO}_2)_5\text{Si}_2\text{O}_9 \cdot 6\text{H}_2\text{O}]$ and uranophane $[\text{Ca}(\text{UO}_2)_2\text{Si}_2\text{O}_7 \cdot 6\text{H}_2\text{O}]$, are stable over a wide range of pH and at the oxidizing conditions prevalent at most uranium waste sites. This method relies on the presence of hydrous calcium silicate (C-S-H) gel as the primary binder in concrete. C-S-H is sparingly soluble and powdered recycled concrete in soil or an aquifer would provide a lasting source of dissolved silica and calcium to promote precipitation of soddyite and/or uranophane. Immobilization of uranium using recycled concrete would be inexpensive, long-lasting, and provide a beneficial reuse of clean concrete from D&D operations.

DGT probes are a relatively new method for measuring the labile, and hence, bioavailable fraction of a metal in soil pore water. A DGT disk consists of an open window plastic casing, a membrane filter, a diffusive gel layer, and a resin gel layer. As ions diffuse through the layers and are accumulated on the resin, the concentration of metals adjacent to the probe decreases, creating a supply of metal ions from the solid phase to the solution. The creation of diffusive supply and release from sediments over time by the DGT disk mimics biotic uptake. Our experiments with decreasing the bioavailability of uranium with recycled concrete provided an excellent opportunity to evaluate DGT probes relative to other methods of measuring bioavailability.

Two sets of experiments were conducted to evaluate different formulations of cement for their effectiveness at decreasing bioavailability of uranium. In the first set of experiments 0.2 grams of cement were mixed into 20 ml of a 1 mg/L (actually 0.98 mg/L) solution of uranium(VI). The mixes were reacted for 24 hours at 40°C (to increase reaction rates). Following reaction, the mixes were filtered through 0.45 μm filters. Five different formulations of cement were used, each with a different amount of silica fume added to Portland cement. The percentage of Portland cement ranged from 100 down to 15 and each was allowed to hydrate for 20 days. Experiments were run with the initial uranium solution at pH of 3.8 and 5.8. At the end of the mixing all samples were adjusted to a pH between 6 and 7 prior to filtering. Controls were run in the same way without the addition of cement. The filtrates were acidified and analyzed for uranium by ICP-MS.

The second set of experiments consisted of two in which the 15% and 60% Portland cement formulations were mixed into uranium contaminated soils from Tim's Branch on the Savannah River Site. Previous work by Knox determined the average uranium concentration of this sample of Tim's Branch soil is 26.5 mg/kg. Samples of the soil weighing 20 grams dry were dampened with DI water and 0.2 grams of each cement formulation were mixed into the 20 gram soil samples. The samples were kept at 100% humidity and mixed frequently for 45 days. The aged samples were analyzed for bioavailability of uranium by four methods – a sequential extraction, extractions with citric acid and EDTA, and the DGT probes.

Analysis of the filtrates in the solution experiments indicated that significant uranium sorbed to the reaction vessels and/or the filters. The filters with the reacted dried cement were retained, but the reaction vessels had been disposed of prior to receiving the filtrate analyses. To test whether the cement had sequestered uranium, the filters from three of the experiments, bearing the dried cement, were leached with a 0.16M HCl solution. Uranium stock solution adjusted to a pH of 6.9 was passed through a filter as well. The filter itself removed 32% of the uranium from the 0.98 mg/L solution. The amount of uranium removed by the cement formulations was calculated accounting for loss to the filter. There was a direct correlation between the percentage of Portland cement in the formulation and the amount of uranium it removed. The 100%, 60%, and 15% Portland cement formulations removed >37%, >17%, and >0% of the uranium from solution. These are semi-quantitative results because we do not know how much of the uranium was actually removed by sorption to the reaction vessel and the filter. We can surmise that the maximum removed by sorption to labware was approximately 32% from the experiment with the filter alone and the fact that the most silica-rich formulation, when leached, returned 68% of the uranium. Nevertheless, the fact that the pure hydrated Portland cement was the most effective is interesting because the binder in most recycled concrete would be pure hydrated Portland cement.

In the soil experiments, the DGT probes indicate that the 60% formulation reduced bioavailability of uranium by about 66%. The extraction procedures are much more aggressive than the DGT probes, and hence don't show the effects of the cement on uranium. For example, the citric acid leachate contains very high concentrations of calcium, indicating the cement components were dissolved. Uranium shows a direct correlation to calcium in these leachates. The EDTA extractions also show much higher calcium concentrations than the control samples suggesting it is much more aggressive than the DGT probes. Thus, we conclude that the DGT probes provide a more accurate measurement of bioavailability than other common methods.

The experiments performed in this LDRD project indicate that recycled cement has substantial potential for treating soils and groundwater contaminated with uranium. The solution experiments, though semi-quantitative demonstrate that hydrated cement pastes remove uranium from solution. Likewise, the same amendments effectively reduce bioavailability of uranium. Furthermore, we conclude that the DGT probes are an effective method for measuring bioavailability of uranium and other metals and are superior to some other common methods.

Establishing the Potential of the TERAS System for CO₂ Capture and Sequestration, M. B. Gorenssek, M. A. Shadday, G. C. Blount

A novel carbon capture process coupling (deep well) gravity-induced hydrostatic pressure, gas lift pumping, compressed air energy storage (CAES), and waste heat recovery that can remove CO₂ from flue gases at a fraction of the cost of traditional amine solvent-based processes was studied in detail. Named TERAS (Thermal Energy Recovery Aqueous Separation), the process can remove 90% of the CO₂ in flue gas to produce a supercritical CO₂ product of >95% purity, suitable for enhanced oil recovery (EOR). Complete conceptual designs for several carbon capture scenarios were developed and

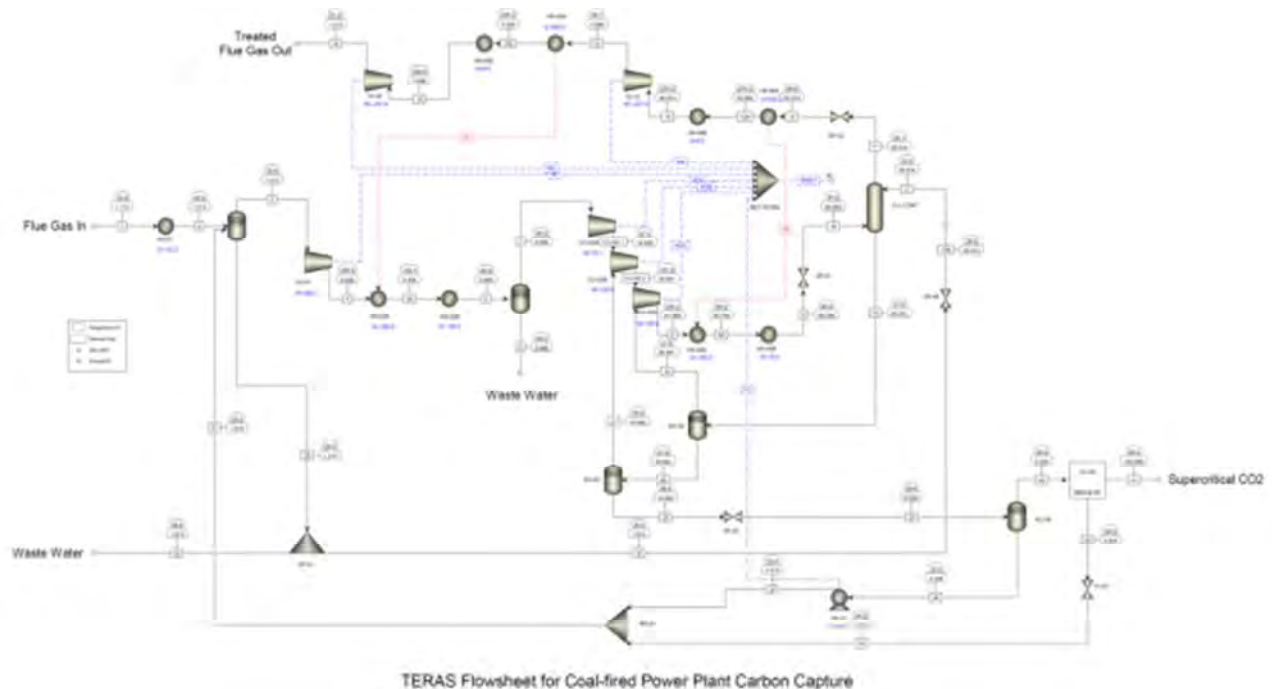
simulated using Aspen Plus. A FORTRAN two-phase drift flux mass transfer model for the well-bore components was also developed and used to confirm the projected capacity for CO₂ separation. The results have already been used to stimulate the interest of potential industrial development partners. We will continue to seek funding for further development using these results as justification.

The objective of this work was to provide a detailed engineering analysis of TERAS by means of simulating the overall process as well as the mass transfer operation at its core to provide concrete evidence of its viability. While nothing is better than an actual physical demonstration, all of the underlying operations can be modeled with a high degree of confidence. The significance of this effort is that it makes a strong case for building a prototype for field demonstration. The results are already being used by an outside consultant (Tetra Tech) to develop a detailed cost estimate for the process as well as a design for absorber and gas/liquid separation modules (under separate funding).

Two parallel paths were pursued: one involved designing and simulating the overall process based on the limiting behavior of the absorber modules; the other consisted of analyzing the mass transfer characteristics of the modules.

Dissolution of CO₂ in water is limited by its solubility, which follows Henry's Law. Consequently, the local equilibrium solubility can be used as an upper limit for CO₂ concentration in the effluent from any given absorber module. This formed the basis of the Aspen Plus process simulations, which found that 8-10 equilibrium stage modules connected in counter-current gas-liquid flow configuration (i.e. co-current flow within individual modules, but connected counter-currently) provide sufficient separation to achieve the target of 90% CO₂ removal at >95% purity. If mass transfer limitations would reduce the effluent concentrations by 50% (a conservative lower limit), then roughly twice as many (16-20) stages would be needed, which is a manageable or practical result.

Aspen Plus simulations were prepared for a variety of flue gas scenarios ranging from 12% to 20% CO₂ concentration, including coal-fired power plants (12-15%) and refinery applications like cracking catalyst decoking/regeneration (20%). Aspen Energy Analyzer was used to perform pinch analyses to optimize energy utilization. The best results (in terms of recuperation) were achieved with two-stage compression of the flue gas feed to the absorber modules and two-stage expansion of the absorber gas effluent, preheating the turbine expander feeds by heat exchange with the compressor effluent streams. For a coal-fired power plant flue gas containing 13% CO₂, the TERAS process required a net energy input of 32.6 MW_e for every 100 MW_e of gross electric power output, which is offset by 9.9 MW_{th} of steam generation. This represents a roughly 29% de-rating of the generating capacity, which compares favorably with the 30% typically quoted for amine solvent-based systems that also have chemical feed and waste disposal costs to consider. With water as the solvent, and no toxic waste by-product, TERAS is an attractive alternative to established carbon capture technologies.



The FORTRAN mass transfer model simulates the dissolution of flue gas constituents in water flowing through absorber modules in a well. The flue gas is assumed to be a mixture of CO_2 and N_2 . Within a single stage or absorption module, the two-phase flow is co-current bubbly downflow, and the gas flow between modules is counter-current. The flue gas is initially injected into the water flowing into the bottom module and the gas removed from the bottom of this module flows upward and is injected into the water flow at the top of the next module as it ascends. This pattern is repeated until gas is finally separated from the flow at the bottom of the top module.

This is a steady-state one-dimensional model. Within a module, the axial distributions of pressure, void fraction, bubble diameter and density, phasic velocities, and dissolved gas concentrations and saturation concentrations are all calculated. Simulation results for a 2,000-ft deep module assembly treating flue from a coal-fired power plant indicate that dissolved CO_2 concentrations well in excess of 50% of saturation are easily attainable.

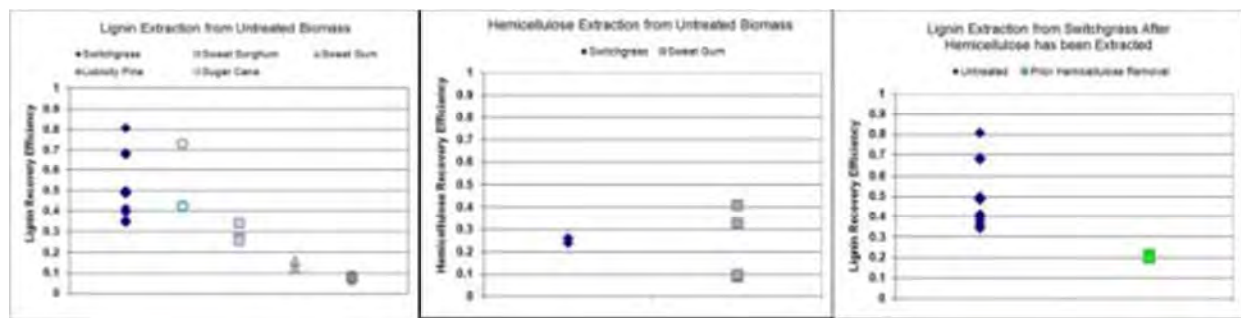
In conclusion, detailed simulations of the TERAS process applied to flue gas from coal-fired power plants and refinery decoking operations have been prepared. These simulations include the overall process flowsheet as well as a detailed model of mass transfer within individual absorber modules. The results indicate that TERAS energy requirements should be comparable to those for amine solvent-based carbon capture processes. However, TERAS does not require the use of chemical solvents (other than pure water) and does not produce any toxic waste by-products. Further analysis is being performed under separate funding by an outside consultant (Tetra Tech). We plan to publish the results of this LDRD in a peer-reviewed journal article, and are actively looking for sponsors to fund development.

Extraction of Hemicellulose and Lignin from Biomass, S. R. Sherman, A. Womack, and J. Goodell

SRNL and Clemson University have been working since 2008 to develop a fermentation-based process for converting lignocellulosic biomass into ethanol. In the process, biomass is treated to separate lignin, and the remaining cellulose and hemicellulose are enzymatically hydrolyzed into fermentable sugars. The yeast used during fermentation prefers cellulosic sugars, and the sugars derived from hemicellulose pass through the fermentation step largely untouched. The process might be more economical if hemicellulose, in addition to the lignin, were separated ahead of the hydrolysis step, because this would provide more options for transforming hemicellulose into higher-value chemicals. This work examined the performance of lignin and hemicellulose extraction methods on different biomass types, and measured the behaviors of extraction steps performed sequentially. It was discovered that extractions performed second in the sequence perform less well than the initial extraction and that the lignin extraction method in particular worked better on grasses than on woody biomass.

Lignin and hemicellulose were extracted from untreated biomass samples, and from samples from which lignin or hemicellulose had previously been extracted, in order to assess the effectiveness of the extraction methods by themselves and when used in a sequence.

Lignin extractions were performed by using the following sequence of steps: 1) Combine 8.5 wt% aqueous NH_4OH with biomass at 8:1 vol:mass ratio and heat for 24 hours at 70-80°C, 2) Filter to remove solids, 3) Boil filtrate until the b.p. reaches 96-98°C to drive off NH_3 , 4) Titrate with H_2SO_4 to reduce pH less than 4, 5) Boil filtrate again until volume falls to about 50% of initial volume, 6) Allow to cool and filter or centrifuge to recover lignin. Hemicellulose extractions were performed using the following sequence of steps: 1) Combine 0.5 wt% aqueous $\text{Ca}(\text{OH})_2$ with biomass at 8:1 volume:mass ratio and heat for 2 to 4 hours at 70°C, 2) Filter to remove solids, 3) Acidify filtrate with H_2SO_4 and mix filtrate with CH_3OH at 1.5:1 vol ratio to precipitate extracted hemicellulose, 4) Centrifuge or filter to recover precipitated hemicellulose.



The lignin extraction method worked best with switchgrass and sugar cane, while the hemicellulose extraction method was statistically indifferent to biomass type. In an extraction process where lignin and hemicellulose were extracted sequentially (in either order), the second extraction was less effective than the first extraction. The lignin extraction method tested is acceptable for use with switchgrass, sugar cane, and sweet sorghum, but it should only be used on untreated biomass. Also, it should not be used on woody biomass such as sweet gum and loblolly pine. The hemicellulose

extraction method is not very effective, even for untreated biomass, and its use is not recommended for future work.

Heterogeneous Materials and Novel Interfaces for Oxygen Separation Membranes, K. Brinkman (SRNL), K. Reifsnider (USC) and A. Virkar (Univ. Utah)

Ceramic membranes are heterogeneous materials which play an essential role in a number of energy conversion related systems including the solid oxide fuel cell (SOFC), oxygen separation and permeation membranes, high temperature electrolysis cells and combustion control sensors. These materials systems have a broad impact across a number of diverse disciplines important to SRNL including energy, tritium processing/operations, homeland security as detection systems and environmental management through off-gassing treatment strategies. Despite the material interest for a variety of applications, fundamental work on the transport properties (electronic, ionic conduction) and surface exchange kinetics as a function of morphology and composition have not been explored to a large extent. The proposed work herein aims to fill this gap by i) synthesizing heterogeneous materials with novel interfaces, ii) experimentally evaluating their transport properties in a unique fashion resulting in enhanced understanding of ionic, electronic conductivity as well as surface exchange kinetics that control membrane separation performance.

Ceramic membranes which transport oxygen ions play an essential role in a number of energy conversion related systems including the solid oxide fuel cell (SOFC), oxygen separation and permeation membranes, high temperature electrolysis cells and combustion control sensors. For the electrolyte functions, the membranes must transport oxygen ions only. On the other hand, permeation membranes, typically used in combustion devices to support oxy-fuel combustion or for partial oxidation reactions involving the production of synthesis gases, require mixed oxygen ion and electronic conduction (MIEC). Traditionally the tailoring of the ratio of ionic conductivity to the materials electronic conductivity, measured as the transference number, has been accomplished by the introduction of aliovalent doping elements creating point defects in the material facilitating the diffusion of charged species. However, several decades of research have not yet produced single phase materials which possess the concomitant ionic and electronic conductivity required for use in membrane separation applications. It is clear that novel “dual phase” heterogeneous materials will be required and that the surface reactions of these materials will be of particular importance as the industry moves toward thin films membranes. This project explored several ionic and electronic conducting material combinations.

Composite MIEC membranes will consist of two contiguous phases, an ion-conducting phase and an electronic conducting phase. The candidate phases should be mechanically and chemically stable at elevated temperature and large oxygen partial pressure gradients. Transport (permeation) of oxygen occurs as a coupled transport of ions and electrons. The overall process is divided into three steps: (a) $\frac{1}{2}\text{O}_2(\text{g}) + 2\text{e}'(\text{M}) \rightarrow \text{O}^{2-}(\text{I})$ at one surface, (b) Coupled transport of O^{2-} and $2\text{e}'$ in opposite directions through the bulk, and (c) $\text{O}^{2-}(\text{I}) \rightarrow \frac{1}{2}\text{O}_2(\text{g}) + 2\text{e}'(\text{M})$ at the other surface. Building on our prior work, the boundary value problems for charge distribution were set and solved with

appropriate boundary conditions and constitutive equations on local morphology features in order to capture the explicit effects of local morphology on the functionality of the MIEC films.

Conventional ceramic powder processing was used for synthesis in order to combine electronic conductive and ionic conductive phases. Figure 1 a) displays a schematic of the dual phase membrane material concept for oxygen separation indicating phase specific electron and ion transport. Figure 1 b) displays X-ray tomography results revealing internal and surface morphology of a sintered YSZ-SrTiO₃ dual phase membrane. Figure 1 c) displays the characterization of conductivity by impedance spectroscopy. The imaginary versus the real impedance as a function of frequency is plotted for Gd doped CeO₂ ionic conductive materials at 400°C; the x axis intercepts and semicircle width gives characteristics of interfacial contributions to conductivity. Ultimately, ion and electronic conductivity give rise to oxygen transport at elevated temperature under a partial pressure gradient. Figure 1 d) displays the oxygen flux (J mol/cm²s) versus temperature for a mixture of 60% volume Gd doped CeO₂ and 40% volume CoFe₂O₄.

A number of material combinations were synthesized and characterized including YSZ, Gd doped CeO₂, SrTiO₃, La_{0.6}Sr_{0.4}CoO₃ and CoFe₂O₄. Surface and internal morphology of dual phase samples were characterized by X-ray tomography. Impedance spectroscopy was used to experimentally evaluate the conductivity of materials combined with broad band dielectric spectroscopy which probed permittivity. Conductivity and permittivity from experiment were used in conjunction with X-ray morphology to set boundary conditions; electromagnetic equations were solved in COMSOL which showed good comparison between measured and calculated impedance as a function of morphology. Optimized CGO-CoFe₂O₄ composite membrane was fabricated and oxygen permeation confirmed. Further work is suggested to extend the interface concept to surface exchange layers and local material interfaces that control the electron/ion surface kinetics and bulk transport.

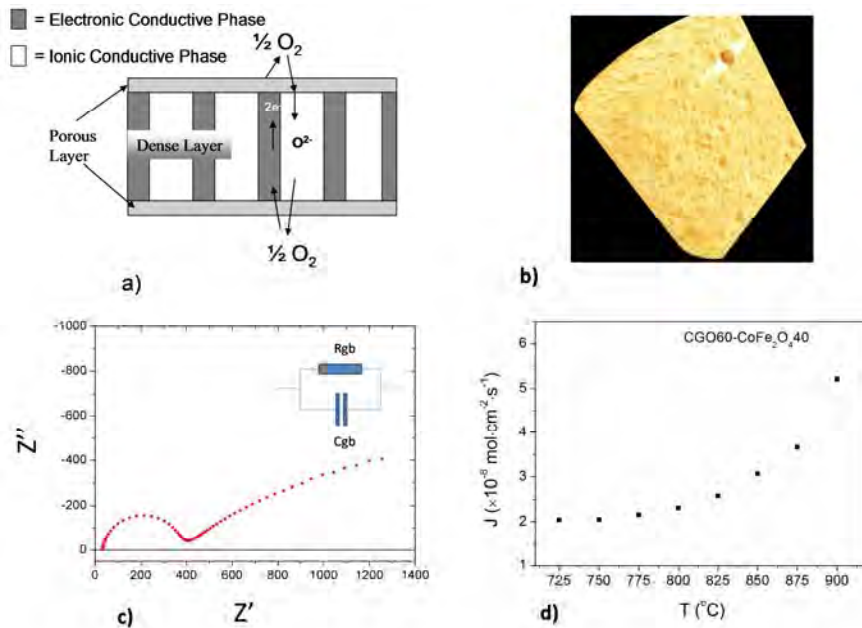


Figure 1. a) Schematic of heterogeneous oxygen separation membrane functionality composed of ionic conductor and electronic conductor, b) X-ray tomography of YSZ-SrTiO₃ composite membrane, c) conductivity characterization of Gd doped CeO₂ material and d) measurement of oxygen flux J (mol/cm²s) versus temperature for a CGO-CoFe₂O₄ composite membrane fabricated in this project.

High Performance Nanofluidic Sensors for Detecting Chemical and Biological Agents in Deterrence of Terrorist Attacks, P.S. Lam, A. Méndez Torres, R. Torres, D. Hathcock, Prof. G. Wang (USC)

Existing technologies for CWA and BWA detection have limited sensitivity, and are slow, expensive and fail to meet several criteria necessary for continuous monitoring and evaluation. To ensure early detectability, devices capable of high sensitivity for ultra-trace element measurement will be developed with the technologies based on recent advances in nano- and micro-fluidics for nano-scale detection. Recent progress in nano- and micro-fluidics has provided the underlying technical foundations for developing a high fidelity nanoscale detection technology for chemical and biological sensors at a low cost. The Savannah River National Laboratory (SRNL) in collaboration with the University of South Carolina (USC) has initiated a program for the development of fluidic sensors. The investigation of nanofluidics technology would provide for ultrahigh sensitivity, selectivity and fast response times in portable and field deployable devices

Our objective is to develop a nanofluidic sensing device based on nanoelectrokinetics, where electric field generated by the electric double layer in the field of the entrance of a nanochannel will cause an electrostatic force on the same charged molecular. In this device, the hydrodynamic force due to fluid flow and electrostatic force compete from each other. The technical approach pursued included (i) measurement of flow velocity using laser photobleaching technique, (ii) fabrication prototypic components using atomic force microscopy and glass tubing pulling, and (iii) numerical simulation for computational prototyping to optimize key parameters in fabricating sensors. Flow velocity was measured with USC recently developed nanovelocimeter. The flow velocity can be determined by measuring the fluorescence directly through a calibration relationship between them. To test selectivity and detection capabilities for different preconcentration, it is very important to know how this preconcentrated is stretched under shear stress and how the concentration of specific agent influence the stretching process under various shear force conditions in microchannel, which has the similar size as those in the entrance of a nanochannel. For this purpose, we measured the flow velocity profiles, in a microcapillary with ID equals to 50 microns, under various concentrations using DNA as a biological surrogate. Fig.1 (a) shows the fluorescence intensity distribution and velocity distribution measured. As shown in the figure, the shape of distribution curve keep the same although the concentration of DNA changes. However, the peak of fluorescence intensity decreases with the increase of DNA concentration. Fig. 1(b) indicates that the velocity profiles keep approximately the same if the volume rate was set as a constant in the experiments. Therefore in the microcapillary of 50 μm in diameter, the DNA within the concentration range studied in this work seems does not change the flow velocity profile.

Atomic force microscopy (AFM) was studied for its potential as a low-cost alternative for the machining of disposable nanochannels. The small AFM tip diameter ($< 10 \text{ nm}$) allows for features at scales restricted by conventional optical and electron-beam lithography. Figure 2 shows an AFM height image of a nanolithography pattern fabricated on a poly(methyl methacrylate) film deposited on glass by spin-coating (DI Multimode AFM). The technique results in well-developed microscale wells and connecting nanochannels. As evidenced by the large material pile-up in the

height image, future work is needed to allow for the efficient displacement of the removed debris from the pattern.

Modeling and finite element analysis simulation was performed to assess the material deformation during fabrication and to simulate AFM tip/coating interaction for (1) benchmarking micro/nano-fabrication of fluidic channels, and (2) optimizing parameters for micro/nano-fabrication. This task took in consideration mechanical properties and fracture/failure criteria, and (2) numerical scheme to model material penetration and scribing. Figure 3 (A-C) shows Finite element simulation of nanofabrication using AFM, contours show stress distribution in MPa, or pico-Newton/nanometer².

The underlying technical foundations for developing a high fidelity nanoscale detection technology for radionuclides at a low cost based on nano-fluidics was investigated in this work. Flow velocity profiles using a biological surrogate were demonstrated showing the possibility to develop highly sensitive detection system. In addition nano device fabrication was studied using both glass tubing and AFM. AFM nanolithography results in a better resolution in the nanoscale and it was demonstrate the ability to mechanically scribe nanochannels on soft polymer samples. Nanofluidic devices offer a means of integrating electrochemical and optical sensing on the same device platform, for verification and monitoring of aqueous solutions. The technology would provide for ultrahigh sensitivity, selectivity and fast response times in portable and field deployable devices.

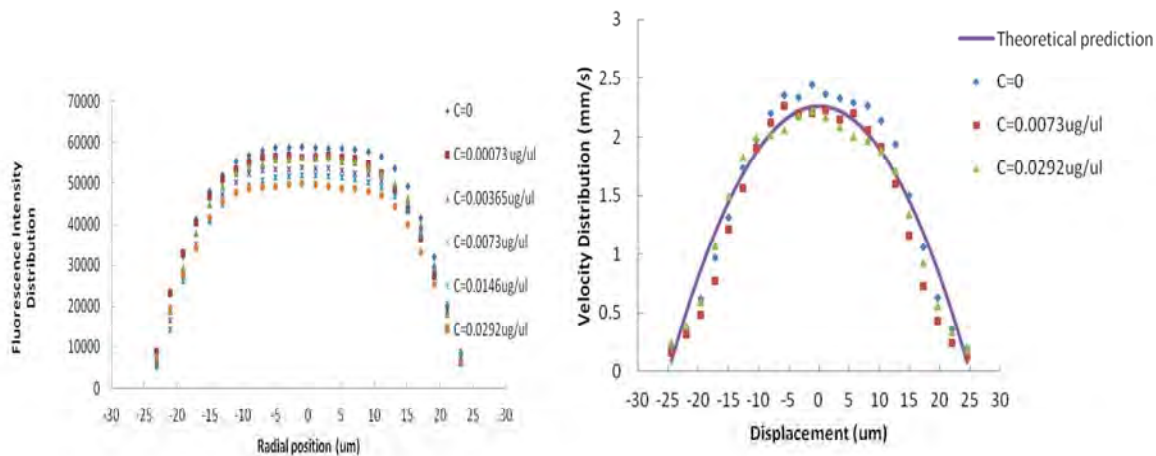


Figure1. Fluorescence Intensity Distribution (left) and velocity distribution (right)

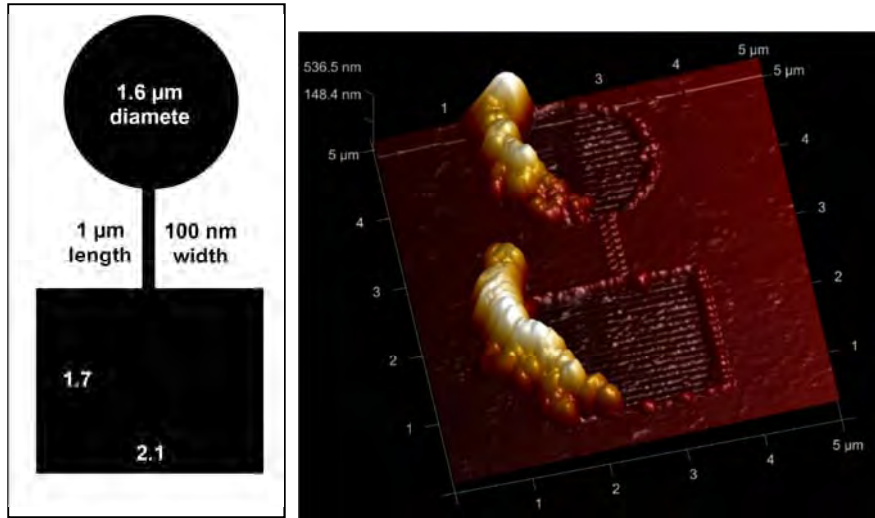


Figure 2. Nanofluidic device pattern fabricated on a PMMA film. Left: Pattern sketch incorporates both microscale fluid reservoirs and a nanochannel. Right:

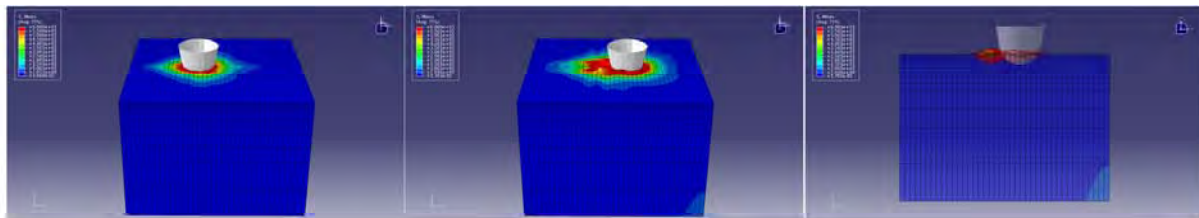


Figure 3. (a) AFM tip has penetrated 5 nanometers into PMMA. (b) AFM tip has scribed 20 nanometers through PMMA (c) Translucent side view showing the materials accumulated outside the scribing path and the material deformation under the moving AFM tip.

Improved Characterization of Air Emission Sources Using Evolutionary Ensembles, *R.L. Buckley, S. R. Chiswell, D.W. Werth, and B. L. O'Steen*

Evolutionary programming (EP) ensembles have been shown to be important in minimizing atmospheric model errors over the first several days of a forecast. This research has explored the usefulness of EP ensembles by creating an operational short-term forecast for the southeast United States with 32 members, updated daily over five months. With the EP technique, input parameters used in the best-performing member for each day are perturbed in the subsequent simulation. Ensembles have been shown to extend the time over which model predictive skill is demonstrated; hence, their use in transport applications (e.g. hazardous releases) can improve the decision making process during emergency situations. Comparisons of the EP ensemble with available initial condition (IC) based ensembles reveal that the EP ensemble generally outperforms the IC ensemble for both temperature and wind speed for inland locations. The latter result is significant for transport applications.

This project developed EP techniques to create an ensemble meteorological dataset in an operational setting. Once the EP forecast generation began, we explored differences between the

typical IC-based ensembles and the new EP-based ensembles. In addition, the ensemble members were used in an atmospheric transport and dispersion model to assess the plume spread for a given scenario, allowing for quantification of plume location uncertainty. The application of these results to transport simulations is important to WFO sponsors with potential customers in NA-22 (non-proliferation), the aviation industry (commercial sector), and the DHS (emergency response). A possible proposal to NA-22 using the EP technique in a western US location is currently being pursued.

This research combines the EP technique with ensemble modeling to provide a short-term 32-member EP-ensemble forecast in an operational setting. In the first phase, the Regional Atmospheric Modeling System (RAMS) was modified to allow for the generation of an ensemble of meteorological forecasts by perturbing input parameters related to topography, incoming solar radiation, and surface conditions. In the second phase of the project, the EP ensemble was evaluated against the standard IC-based ensemble by using an independent set of observation locations to examine differences in winds and temperature. In addition, identification of the meteorological parameters leading to the largest variability between ensemble members was examined. Finally, the EP ensemble meteorology data was input to a Lagrangian particle dispersion model to examine uncertainty in transport output based on the EP members.

The operational setting itself required establishment of a domain covering the southeast United States, tools to objectively perturb the initial RAMS parameters, defining observation locations to rank which of the 32 simulations performed best for a given day, developing tools to “score” the simulations relative to these observations (using RMS error of wind speed, wind direction, temperature, and dew-point temperature), and scripts to automate the process. In the second phase of the project, analysis tools were developed to examine how well the ensemble generated a spread in results (i.e. Talagrand diagrams). It was shown that the spread initially was not large enough, so the range of input parameter perturbations was arbitrarily doubled. Although some improvement in the spread was gained, further analysis of which parameters are of most importance is still required. The RAMS configurations initially relied on climatological sea surface temperatures, resulting in a bias over ocean areas due to an anomalously warm western Atlantic region which the short-term model forecasts could not overcome. The introduction of observed sea surface temperatures successfully eliminated the model bias and further improved thermally driven ocean-land circulations in the model.

The five-month period of analysis has helped show which input parameters influence the skill of the model. These include (relative to standard default inputs) higher input values for topography enhancement, higher minimum vertical velocity required for convective precipitation formation, higher surface albedo (both wet and dry), and relatively weaker nudging by large-scale data at both lateral boundary and the interior model domain. The forecasting skill comparison between EP and IC ensembles was performed at four different times of day (8am, 2pm, 8pm, and 2am) and showed some improvement in temperature forecasts with EP for inland locations. Even better improvement in wind speed skill was shown at all times when using the EP ensembles.

Finally, the EP ensemble forecast members were used in determining uncertainty in surface concentration using a Lagrangian particle dispersion model, assuming a hypothetical, continuous

release from SRS. Areas were defined showing the percentage of transport simulations predicting concentration exceeding a threshold value. Higher agreement among plume results implies further confidence in the transport results. A comparison of transport results for both the EP and IC ensembles for a given forecast day was generated and results indicate more spread in the IC ensemble. This result is not surprising given that several different models were used in the generation of the IC ensemble, whereas the EP ensemble is working from a single model, RAMS.

The EP ensemble has been shown to generally outperform the standard IC ensemble for the southeast United States for the spring and summer months studied in this research. In particular, improvements in temperature and wind forecasts were seen to be greatest over the land areas of the model domain where variations in topography, vegetation, soil and moisture are capable of affecting model conditions more rapidly than ocean areas, which present a more homogeneous lower boundary. In comparison to land temperatures, the sea surface temperature varies much more slowly with a smaller diurnal range. Consequently, both the EP and IC ensembles exhibit more uniformity during the period of model simulation over ocean areas. Additionally, the EP ensemble shows increasing improvement with forecast time compared to the IC ensemble for the duration of the forecast period, which is attributable to the decreasing influence of the initial model conditions common to both ensembles. It is important to note that although the analysis is applied to the southeast United States in this research, the technique can be applied anywhere in the world. The EP method lends itself to tuning model inputs specific to different regions. The trends in the best-performing parameter values indicate a few that could be important in improving forecasting capability. The application of the ensemble meteorology to transport and dispersion calculations reveals a larger spread in plume predictions (i.e. less certainty) for those days with inland (i.e. southeasterly) directed surface winds, as well as for periods with strongly varying wind directions. By applying the EP ensemble to transport applications in an operational setting, we have demonstrated an improvement in characterizing air-emission sources. Further demonstration of the technique during the autumn and winter seasons is planned using existing infrastructure, with further analysis of trends. In addition, a presentation of these results at an upcoming American Meteorological Society annual meeting will occur in February 2012, as well as anticipated publication in a peer-reviewed journal article in the upcoming fiscal year.

Ionogels as Solid Electrolytes for Advanced Battery Applications, *B. Garcia-Diaz, J. Gray, A. Visser, M. Au, J. Weidner, K. Zeigler, and T. Adams*

Commercial hybrid electric vehicles (HEV) including the plug-in hybrid electric vehicles (PHEV) serve as a potential means to reduce the nation's dependence on oil and environmental pollution. Current vehicles use nickel metal hydride (NiMH) rechargeable batteries and Li-ion rechargeable batteries (LIBs) are being developed for increased energy density. The development of a solid ionic liquid based electrolyte (ionogels) for use in advanced batteries offers a novel solution to many weaknesses characteristic of current battery electrolytes, including corrosion problems that currently limit the power and lifetime of batteries and high volatility while forming a compact solid layer that is inherently more easily processed than a liquid phase. Ionic liquids and ionogels have many qualities

that make them excellent candidates for battery electrolytes, including low chemical reactivity with typical electrode materials, negligible vapor pressure and flammability with ionic and electric conductivities that can be tailored for specific applications. The success of these ionogel electrolyte batteries relies in demonstrating sufficient ionic conductivity while retaining the compatibility with the other battery components. Ionogels have been synthesized using a number of ionic liquids and supporting polymeric phases chosen for electrochemical, physical and chemical properties and compared to literature standards for current battery technologies.

A critical issue for batteries regardless of the underlying chemistry is the potential for severe corrosion of the electrode materials in aggressive electrolyte solutions. This can result in a drastic decrease in battery charge capacity after a few charge/discharge cycles. Additionally, many commercial battery electrolytes are volatile organic solvents which can result in potential safety concerns with runaway thermal reactions leading to fire hazards. The focal point of the research reported is to synthesize and test improved ionogel electrolytes made by combining ionic liquids with selected supporting polymeric materials. The formation of the gel forms of these ionic liquids makes them easier to process from an engineering standpoint, and might allow thinner electrochemical cells to be incorporated into battery technologies, thus enabling the trend towards more compact energy storage.

The areas where ionogel electrolytes need improvement for Li-ion battery applications are porosity, mechanical strength, and lithium mobility. The project focused on identifying and testing membrane synthesis methods to improve these three aspects of ionogel performance. The most basic aspect of improving ionogel membrane performance is to improve the porosity and pore structure of the membrane. Separators in battery applications are inert to chemical reaction and provide a physical barrier that allows the electrolyte to pass while preventing contact of the electrodes. Ionic liquids serve as the electrolyte in ionogel membranes and are highly stable, but have ionic conductivities that are lower than carbonate electrolytes and the presence of the inert membrane further reduces the conductivity. The simplest method to increase the ionic conductivity in ionogel membrane is to increase the porosity of the membrane to allow more free transport of the electrolyte. To achieve increased porosity with regular pore structure, a dual polymer template was used during the casting of a polyvinylidene fluoride – hexafluoropropylene (PVDF-HFP) matrix. The method used a crystalline water soluble polymer with a surfactant to provide a uniform pore structure. Both of the polymers had previously been shown to have a positive effect on ionic conductivity and were chosen so that trace contamination due to incomplete removal would not decrease electrochemical performance. The membranes synthesized using this method had a porosity of 75% as measured by the uptake of butanol into the membrane pores. The membrane structure and a DMA showing a typical glass transition temperature of -37°C for PVDF-HFP. It should be noted that the loss modulus for the polymer was less pronounced than for typical PP separators for Li-ion batteries. SEM images and DMA characterization of the baseline polymer are shown in Figure 1 a) and b). Oxygen, an element only present in the template polymers, was found by EDX to only be 1% by weight in the membrane suggesting near complete removal of the template polymers

Increasing membrane porosity requires increased mechanical strength for the remaining polymer. Bismalimide (BMI) was used as a cross linking agent in the current study due to its high mechanical strength and its double bonded oxygen groups that can promote ionic conductivity. Figure 1 c) shows an SEM image of the pores in the cross-linked membrane. The cross-linking of the membrane leads to higher oxygen content in the membrane from the 10 wt% BMI and also from potentially increased trapping of PVA and surfactant polymers.

Silica filler was incorporated into the PVDF-HFP membranes to improve the transference number of lithium ions in the PVDF-HFP membrane. Membranes were synthesized with 5 wt% and 10 wt% silica. Figure 1 d) shows an SEM image of a membrane with 10 wt% of the silica filler. The 10 wt% silica membranes appear to show agglomeration of particles. The average particle size for the fumed silica was 7 nm, but the SEM showed larger particles that were mostly composed of silicon and oxygen. Lower weight loadings showed more consistent membrane composition.

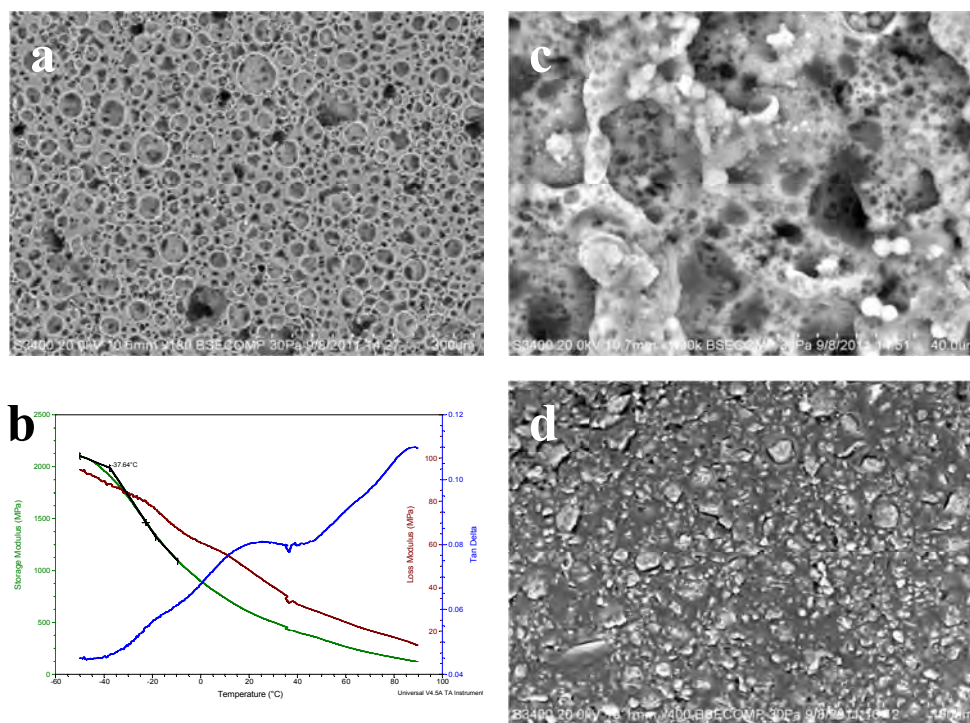


Figure 1. Characterizations of Novel Ionogel Matrix Membranes: a) SEM of a baseline MEA using the “tri-polymer” method, b) DMA results for the baseline ionogel membrane, c) SEM of a bismaleimide crosslinked membrane, and d) a baseline membrane with 10 wt% fumed silica filler

Organic-based Ionic Salts for the Optimization of Alkaline Fuel Cells, *E. B. Fox (PI), H.R. Colón-Mercado, A.E. Visser, N. J. Bridges, C. W. James, and W. Ho (Ohio State)*

Alkaline fuel cell (AFC) operation is currently limited to specialty applications such as low temperatures and pure H₂/O₂ due to the corrosive nature of the electrolyte and formation of carbonates. This work will develop new electrolytes that are less corrosive, have higher operating temperatures, and enable alternative fuels. AFCs are the cheapest and potentially most efficient (approaching 70%) fuel cells. The fact that non-Pt catalysts can be used, makes them an ideal low cost

alternative for power production. The anode and cathode are separated by and solid electrolyte or alkaline porous media saturated with KOH. However, CO₂ from the atmosphere or fuel feed severely poisons the electrolyte by forming insoluble carbonates. The corrosivity of KOH (electrolyte) limits operating temperatures to no more than 80°C. This work will focus on the examination of ionic liquids as electrolyte solutions for the replacement of KOH because they do not chemically bond to CO₂. Low corrosivity and negligible vapor pressures of the IL will allow the operation at high temperatures. This approach is novel as it targets the root of the problem (the electrolyte) unlike other current work in alkaline fuel cells which focus on making the fuel cell components more durable.

AFCs differ from typical proton exchange membrane fuel cells (PEMFC) in that the reactions occur in a basic environment. Because the electrolyte is basic, oxygen at the cathode is reduced to hydroxide ions that are transported through the cell to the anode where they combine with hydrogen to produce water. Because of the basic nature, slow reactions, such as those at the cathode can occur at faster rates, eliminating kinetic limitations that typically affect PEMFCs. This fact proves advantageous enabling the use of alternative electrocatalysts to Pt at the cathode electrode. Typically AFCs operate at low temperatures due to the corrosive nature of the electrolyte, which could be dissolved KOH or solid polymer hydroxide ions conductors. The use of new solid conductors has created renewed interest in AFCs. They enable the use of air, instead of pure oxygen, without the detrimental effects typically seen from the binding of CO₂ present in air with the hydroxide salts forming insoluble carbonates. However, solid proton conductors still have major limitations in temperatures, stabilities, conductivities, and manufacturability. In this work we began studying a new and un-explored alternative route to solving all of the issues plaguing AFCs, which consists on the use of stable easy to manufacture polymers impregnated with ionic liquids.

ILs are salts, in the liquid state, designed to have weak intra-molecule interactions between the cation and anion lowering the salt's melting point below 100°C. This weak ion association is highly desired in electrolytes, as the more dissociated the electrolyte is, the higher the conductivity of the electrolyte solution and thus the 'easier' for charges to pass from the cathode to the anode. ILs generally have lower ion association than traditional electrolytes (e.g., perchlorate salts). They also have several other benefits, including low corrosivity, and higher operating windows of temperatures and chemical potentials. In addition because of the weak intermolecular interactions, ILs do not form insoluble carbonate species that plaque conventional KOH and NaOH electrolytes in alkaline fuel cells. This work aims to characterize, select, and incorporate different ILs with properties suitable to AFC operation in a hydroxide conducting polymer.

In order to screen potential electrolytes for this study, the IL conductivity will be measured was measured using an ion conductivity probe. Results are found in Figure 1 below. It is seen that the imidazolium cation with shorter chain length provides the highest bulk conductivity, while the bis(trifluoromethylsulfonyl)imide anion provides the highest bulk conductivity.

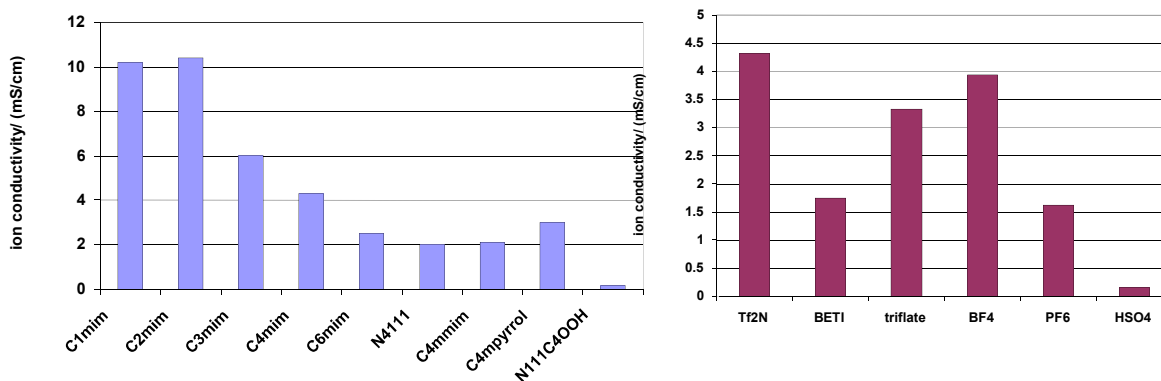


Figure 1: Effect of cation (blue) and anion (red) on ion conductivity of select ionic liquids. The common anion is bis(trifluoromethylsulfonyl)imide (blue) and the common cation is 1-butyl-3-methylimidazolium (red).

Based on these results the [C₄mim][Tf₂N] and [C₄mim][OH] ILs were tested with the RDE under H₂, O₂ and CO₂ for performance. Due to the high viscosity of the [C₄mim][OH] the IL was not able to be tested electrochemically. Electrochemical results for the [Tf₂N] showed typical cyclic voltammograms for the Pt electrode that was being used. The results at room temperature indicate that there is a potential separation of 720 mV between the hydrogen oxidation reaction and the oxygen reduction reaction. No reactions were observed when CO₂ was introduced to the electrolyte. This result indicates that with different IL combinations, it is possible to expand the potential window and will allow for the use of high temperature FC.

OSU synthesized PVA based membranes impregnated with KOH and PBI membranes impregnated with benzalkonium hydroxide which were tested for conductivity using a BeckTech in-plane conductivity test cell at 80 °C and 120 °C. Results for PVA/KOH (70/30) at 80 °C show conductivities starting from 3.6 x 10⁻⁷ S/cm at 0 RH and going up to 1.4 x 10⁻² S/cm at 70%RH. In the case for the PBI/benzalkonium hydroxide (70/30) at 80 °C, the conductivity remains at ~ 10⁻⁷ S/cm regardless of the RH. At temperatures of 120 °C the PVA samples tend to be mechanically unstable. While the PBI sample is stable at higher temperatures, the conductivity remained unchanged.

Metrics

This LDRD funded project resulted in:

- An invited presentation to the AIChE annual meeting in Minneapolis, MN on 10/19/11.
- Employment of one summer intern.
- Establishment of collaboration with Ohio State.
- Submission of a proposal to EERE for \$1M over two years.

Stable Electrocatalysts for High Temperature Fuel Cells, M. C. Elvington, H. R. Colón-Mercado

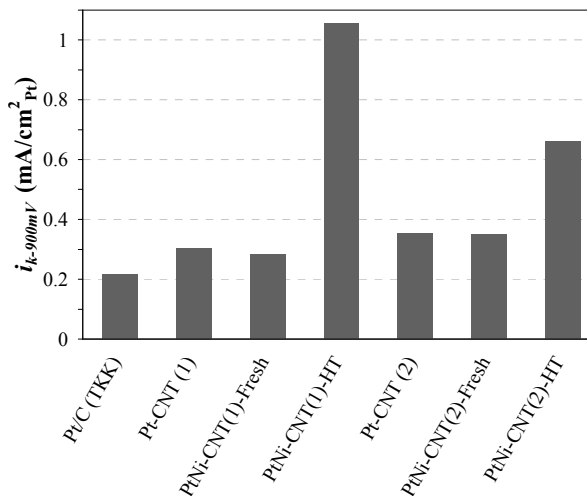
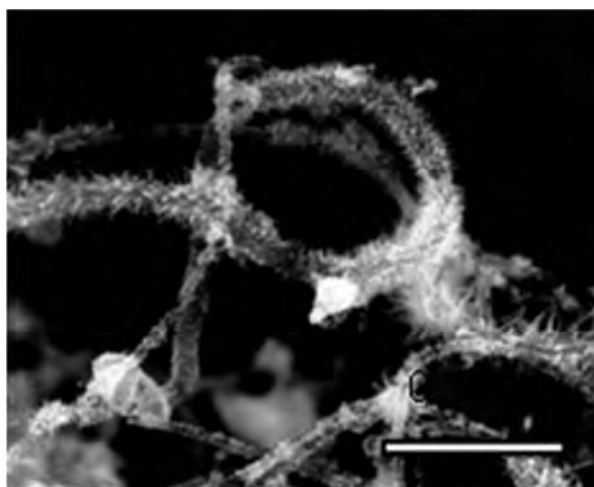
The preparation and characterization of Pt and PtNi electrocatalysts supported on graphitized or nitrogen doped carbon nanotubes is described. The syntheses are simple chemical reactions using a single reducing agent, a platinum or nickel salt precursor, a carbon nanotube support and no surfactant. Pt deposition onto carbon nanotubes (CNT) result in nano-scale Pt needle-like formations as identified by scanning and transmission electron microscopy. Subsequent Ni deposition and heat treatment result in a Pt/Ni alloy that retains its needle-like geometry, however, they are reduced in length and larger in diameter. All Pt and Pt/Ni materials were tested as electrocatalysts for the oxygen reduction reaction (ORR). Electrochemical characterizations included cyclic voltammetry (CV) and rotating disk electrochemistry (RDE). Each of the Pt and Pt/Ni “needle” catalysts tested showed improved performance for the ORR as compared to a commercial Pt/C catalyst, with the heat treated Pt/Ni “needle” catalysts supported on CNT.

The project team investigated the different synthesis methods for creating high activity Pt base nanocatalysts on two different highly stable carbon nanotube supports. The work targeted several weaknesses in state of the art technologies in order to generate the next generation of high temperature electro-catalysts. Initial results indicate the produced catalysts exceed the specific activity target set by DOE for transportation applications at 2015 for stationary power production.

Pt “needles” supported on carbon nanotubes, was derived from a procedure developed by Sun, et al., to deposit Pt “needles” on carbon fibers. The adopted procedure was employed here for the deposition on CNT. A procedure developed by Deivaraj, et al. was adopted and modified for the addition of Ni onto the Pt “needles” supported on CNT. Electrochemical measurements were conducted in a standard three-compartment electrochemical cell at room temperature using a rotating disk electrode (RDE) setup. A high resolution transmission electron microscopy was used to image the lattice of the Pt “needles” and measure the particle diameter. Field emission scanning electron microscope was used to study sample morphology and analyze Pt and Pt/Ni particle size and distribution. X-ray powder diffraction was performed using a PANalytical X’pert Pro to characterize the products, using Cu-K radiation. Compositional analyses of the catalysts were performed using inductive coupled plasma-emission spectroscopy.

The freshly synthesized electrocatalysts show a Pt needlelike structure that is 3.6 nm in diameter and approximately 100 nm in length. When the Pt eletrocatalysts are formed on the CNT support, the growth occurs perpendicular to the surface of the CNT. Note that a carbon support had to be present for the Pt needles to be formed. The figure on the left shows typical FESEM image for the CNT supported Pt needles. After heat treatment, however, the needles increase in thickness. An analysis of the images show that the needles grow from 3.6 nm in diameter to 8 - 11 nm for PtNi/CNT. The ORR activity of the electrocatalysts was measured electrochemically by obtaining linear sweep voltamograms in oxygen-saturated 0.1 M HClO₄ solution. The figure on the right shows the specific activities at 900 mV compared to that of a commercial Pt/C catalyst which had a measured specific activity of 0.22 mA/cm², a value that agrees well with the literature. The

difference in activity between the Pt catalysts with the two different carbon nanotube supports could be attributed to the difference in the Pt to Ni ratio.



Pt base catalysts based were synthesized, characterized and tested for electrochemical activity. The catalysts show nano “needle” formation of the Pt electrocatalysts on carbon nanotubes. The initial electrochemical activity offer much higher specific activity than commercial Pt/C (TKK).